International Journal of Solids and Structures 50 (2013) 4043–4054

Contents lists available at ScienceDirect

International Journal of Solids and Structures

journal homepage: www.elsevier.com/locate/ijsolstr

An incremental variational approach to coupled thermo-mechanical problems in anelastic solids. Application to shape-memory alloys

M. Peigney [a,*], J.P. Seguin [b]

[a] Université Paris-Est, Laboratoire Navier (Ecole des Ponts ParisTech, IFSTTAR, CNRS), F-77447 Marne la Vallée Cedex 2, France
[b] Laboratoire d'Ingénierie des Systèmes de Versailles, Université de Versailles, 45 Avenue des Etats-Unis, 78035 Versailles Cedex, France

ARTICLE INFO

Article history:
Received 27 March 2013
Received in revised form 10 July 2013
Available online 21 August 2013

Keywords:
Incremental variational principles
Thermo-mechanical coupling
Non-smooth mechanics
Shape memory alloys

ABSTRACT

We study the coupled thermo-mechanical problem that is obtained by combining generalized standard materials with Fourier's law for heat conduction. The analysis is conducted in the framework of non-smooth mechanics in order to account for possible constraints on the state variables. This allows models of damage and phase-transformation to be included in the analysis. In view of performing numerical simulations, an incremental thermo-mechanical problem and corresponding variational principles are introduced. Conditions for existence of solutions to the incremental problem are discussed and compared with the isothermal case. The numerical implementation of the proposed approach is studied in detail. In particular, it is shown that the incremental thermo-mechanical problem can be recast as a concave maximization problem and ultimately amounts to solve a sequence of linear thermal problems and purely mechanical (i.e. at a prescribed temperature field) problems. Therefore, using the proposed approach, thermo-mechanical coupling can be implemented with low additional complexity compared to the isothermal case, while still relying on a sound mathematical framework. As an application, thermo-mechanical coupling in shape memory alloys is studied. The influence of the loading strain-rate on the phase transformation and on the overall stress–strain response is investigated, as well as the influence of the thermal boundary conditions. The numerical results obtained by the proposed approach are compared with numerical and experimental results from the literature.

1. Introduction

This paper focuses on coupled thermo-mechanical evolutions of dissipative solids, in the geometrically linear (small strains) setting. The framework of generalized standard materials in non-smooth mechanics is considered (Halphen and Nguyen, 1975; Moreau and Panagiotopoulos, 1988; Frémond, 2002). In that framework, the local state of the material is described by the strain $\boldsymbol{\varepsilon}$, the temperature θ, and an internal variable $\boldsymbol{\alpha}$. The constitutive laws are determined from the Helmholtz free energy w and a convex dissipation potential Φ. In its original form (Halphen and Nguyen, 1975), that framework covers a wide range of elasto–plastic models, including limited and nonlinear hardening. Its extension to non-smooth mechanics has been extensively studied by Frémond (2002) and allows constraints on the internal variable $\boldsymbol{\alpha}$ to be taken into account in a rigorous fashion. That feature is crucial for the modelling of such phenomena as damage or phase-transformation, as the internal variable in such cases is typically bounded. The thermodynamic analysis of the media considered is presented in Section 2, leading to a boundary value problem for the mechanical and thermal fields. As pointed out by Yang et al. (2006), the time-discretization of the thermo-mechanical evolution problem is a sensitive issue because of the coupling between mechanical and thermal equations. For instance, the Euler implicit scheme leads to an incremental thermo-mechanical problem for which existence of solutions cannot generally be ensured. This is in contrast with the isothermal case, for which the Euler implicit scheme provides a well-posed incremental problem under standard assumptions of convexity on the functions w and Φ.

One objective of this paper is to propose a sound time-discretization scheme for coupled thermo-mechanical problems, retaining some essential features displayed by the Euler scheme in the isothermal case (most notably the consistency with the rate problem and the existence of solutions). A central idea is the use of a variational formulation for the incremental problem. Incremental variational principles for dissipative solids have been the focus of a lot of attention in recent years, offering new perspectives in various topics such as finite-strains elasto-viscoplasticity (Ortiz and Stainier, 1999), homogenization (Miehe, 2002; Lahellec and Suquet, 2007), formation and stability of microstructures (Ortiz and Repetto, 1999; Miehe et al., 2004). Incremental variational principles for coupled thermo-mechanical problems have been proposed by Yang et al. (2006) in the case where the heat flux $\boldsymbol{q}$

* Corresponding author. Tel.: +33 1 6415 3746; fax: +33 1 6415 3741.
E-mail address: michael.peigney@polytechnique.org (M. Peigney).

0020-7683/$ - see front matter © 2013 Elsevier Ltd. All rights reserved.
http://dx.doi.org/10.1016/j.ijsolstr.2013.08.013

derives from a potential χ in $(\nabla\theta)/\theta$, i.e. when the heat conduction law takes the form $\boldsymbol{q} = -\chi'((\nabla\theta)/\theta)$. In this paper, we stick with the standard Fourier's law of heat conduction $\boldsymbol{q} = -K\nabla\theta$, which does not fall in the format considered by Yang et al. (2006).

In Section 3 we introduce an incremental problem for the class of coupled thermo-mechanical problems considered, along with a corresponding variational formulation. The variational formulation of the incremental thermo-mechanical problem serves two purposes. First, it allows the existence of solutions to be studied, as discussed in Section 3. Second, the variational formulation leads to a convenient and efficient way of solving the incremental thermo-mechanical problem. The latter can be indeed be recast as a concave maximization problem, for which well-known algorithms are available. As detailed in Section 4, an advantage of that approach is that the solution of the thermo-mechanical problem can be obtained by solving a sequence of linear thermal problems and purely mechanical (i.e. at prescribed temperature) problems. This calls for an easy implementation in an existing finite-element code. A crucial point in the analysis lies in the introduction of an auxiliary linear problem, akin to the adjoint state used in optimal control problems (Lions, 1968).

As an application, the proposed method is used in Section 5 to study thermo-mechanical coupling in shape-memory alloys. The significant role of thermal effects in shape-memory alloys has notably been put forward by Peyroux et al. (1998) and Chrysochoos et al. (2003). The solid/solid phase transformation that occurs in those materials is known to produce significant amounts of heat, associated both with recoverable latent heat effects and irreversible frictional contributions. Depending on the rate of loading and on the thermal exchange conditions, the heat produced by the phase transformation may not have time to diffuse in the body and the temperature field may become inhomogeneous. In such conditions, the overall stress–strain response becomes significantly different from its isothermal counterpart, and it is mandatory to take the thermo-mechanical coupling into account. Therefore, shape-memory alloys offer a particularly relevant application of the general methods presented in this paper. In Section 5, the influence of thermal effects on the phase-transformation and on the overall stress–strain curve is investigated in detail.

2. Thermo-mechanical evolutions of continuous media

2.1. Thermodynamic principles

Consider the evolution (on a time interval $[0,T]$) of a continuous medium occupying a domain Ω in the reference configuration. We restrict our attention to the geometrically linear setting, defining the strain $\boldsymbol{\varepsilon}$ as $\boldsymbol{\varepsilon} = 1/2(\nabla\boldsymbol{u} + \nabla^T\boldsymbol{u})$ where $\boldsymbol{u}$ is the displacement. The first principle of thermodynamics gives

$$\int_t^{t'} \dot{E}d\tau + \int_t^{t'} \dot{K}d\tau = \int_t^{t'} Pd\tau + \int_t^{t'} \mathring{Q}dt \text{ for all } 0 \leqslant t \leqslant t' \leqslant T. \quad (1)$$

In Eq. (1), K and E are respectively the kinetic and the internal energy of the system. The internal energy E can be written in the form $E = \int_\Omega e d\boldsymbol{x}$ where e is the internal energy density. In the right-hand side of (1), P denotes the power of external loads, and $\mathring{Q}$ is the rate of heat received by the system. The upper dot in (1) denotes left-time derivative.[1] The principle of virtual power gives the relation

$$\dot{K} = P - \int_\Omega \boldsymbol{\sigma} : \dot{\boldsymbol{\varepsilon}} d\omega \quad (2)$$

where $\boldsymbol{\sigma}$ is the stress. Expressing $\mathring{Q}$ as

$$\mathring{Q} = -\int_{\partial\Omega} \boldsymbol{q}.\boldsymbol{n} d\omega + \int_\Omega r d\omega \quad (3)$$

where $\boldsymbol{q}$ is the heat flux and r a heat source, the relation (1) can be rewritten as

$$\int_t^{t'} \int_\Omega (\dot{e} - \boldsymbol{\sigma} : \dot{\boldsymbol{\varepsilon}} + \operatorname{div}\boldsymbol{q} - r)\, d\omega d\tau = 0 \text{ for all } 0 \leqslant t \leqslant t' \leqslant T. \quad (4)$$

The relation (4) also holds when replacing Ω with an arbitrary subdomain $\Omega' \subset \Omega$. Therefore, we obtain the local equation

$$\dot{e} - \boldsymbol{\sigma} : \dot{\boldsymbol{\varepsilon}} + \operatorname{div}\boldsymbol{q} - r = 0 \text{ a.e. in } \Omega \times [0,T] \quad (5)$$

where the abbreviation 'a.e' stands for 'almost everywhere'. The second principle of thermodynamics gives

$$\int_t^{t'} \int_\Omega \dot{s}\, d\omega d\tau \geqslant \int_t^{t'} \int_\Omega \frac{r}{\theta} - \operatorname{div}\frac{\boldsymbol{q}}{\theta}\, d\omega d\tau$$

where s is the entropy density and θ is the local temperature. Using a similar reasoning as above, we obtain the relation

$$\theta\dot{s} - r + \operatorname{div}\boldsymbol{q} - \boldsymbol{q}.\frac{\nabla\theta}{\theta} \geqslant 0 \text{ a.e. in } \Omega \times [0,T].$$

Making the classical assumption of separation between the intrinsic dissipation $\theta\dot{s} - r + \operatorname{div}\boldsymbol{q}$ and the thermal dissipation $-\boldsymbol{q}.(\nabla\theta)/\theta$, we obtain the inequalities $-\boldsymbol{q}.(\nabla\theta)/\theta \geqslant 0$ and

$$\theta\dot{s} - r + \operatorname{div}\boldsymbol{q} \geqslant 0 \text{ a.e. in } \Omega \times [0,T]. \quad (6)$$

Eqs. (5),(6) can be rewritten in terms of the Helmholtz free energy density $w = e - \theta s$ as

$$\dot{w} + \theta\dot{s} + s\dot{\theta} = \boldsymbol{\sigma} : \dot{\boldsymbol{\varepsilon}} + r - \operatorname{div}\boldsymbol{q} \text{ a.e. in } \Omega \times [0,T], \quad (7)$$

$$\boldsymbol{\sigma} : \dot{\boldsymbol{\varepsilon}} - s\dot{\theta} - \dot{w} \geqslant 0 \text{ a.e. in } \Omega \times [0,T]. \quad (8)$$

2.2. Mechanical constitutive laws

In the framework of standard generalized materials (Halphen and Nguyen, 1975), the local state of the material is described by the strain $\boldsymbol{\varepsilon}$, the temperature θ, and an internal variable $\boldsymbol{\alpha}$ living in a vectorial space denoted by $\mathbb{A}$. The constitutive laws are determined by the Helmholtz free energy $w(\boldsymbol{\varepsilon}, \boldsymbol{\alpha}, \theta)$ and a convex dissipation potential $\Phi(\dot{\boldsymbol{\alpha}})$ according to the following relations:

$$\boldsymbol{\sigma} = \frac{\partial w}{\partial \boldsymbol{\varepsilon}}, \quad (9.1)$$

$$\boldsymbol{A} = -\frac{\partial w}{\partial \boldsymbol{\alpha}}, \quad (9.2)$$

$$s = -\frac{\partial w}{\partial \theta}, \quad (9.3)$$

$$\boldsymbol{A} \in \partial\Phi(\dot{\boldsymbol{\alpha}}), \quad (9.4)$$

where ∂ denotes the subdifferential operator. Recall (Brézis, 1972) that the subdifferential ∂f of a function $f : \mathbb{A} \mapsto \mathbb{R}$ is the multi-valued mapping defined by

$$\partial f(\boldsymbol{x}) = \{\boldsymbol{\tau} \in \mathbb{A} | f(\boldsymbol{y}) - f(\boldsymbol{x}) \geqslant \boldsymbol{\tau}.(\boldsymbol{y} - \boldsymbol{x})\ \forall \boldsymbol{y} \in \mathbb{A}\}. \quad (10)$$

In the following, the dissipative behaviour is assumed to be *rate-independent*. In such case, the dissipation potential Φ is positively homogeneous of degree 1, i.e. satisfies

$$\Phi(\lambda\dot{\boldsymbol{\alpha}}) = \lambda\Phi(\dot{\boldsymbol{\alpha}}) \text{ for any } \lambda \in \mathbb{R}^+ \text{ and } \dot{\boldsymbol{\alpha}} \in \mathbb{A}. \quad (11)$$

[1] In non-smooth mechanics, left- and right-time derivative of physical quantities may not be equal. In order to respect the principle of causality, the constitutive relations need to be written in terms of left-time derivatives (see e.g. Frémond, 2002).

The property (11) obviously implies that $\Phi(0) = 0$. Moreover, combining (11) with the convexity of Φ, it can easily be shown that $\Phi(\dot{\boldsymbol{\alpha}})$ is positive for all $\dot{\boldsymbol{\alpha}}$. For latter reference, we note the following property that is a direct consequence of (10) and (11):

$$\partial\Phi(\lambda\dot{\boldsymbol{\alpha}}) = \partial\Phi(\dot{\boldsymbol{\alpha}}) \text{ for any } \lambda \in \mathbb{R}^+ \text{ and } \dot{\boldsymbol{\alpha}} \in \mathbb{A}. \tag{12}$$

Note that the constitutive laws (9) satisfy the inequality (8). From (9) we have indeed

$$\boldsymbol{\sigma} : \dot{\boldsymbol{\varepsilon}} - s\dot{\theta} - \dot{w} = \boldsymbol{A}.\dot{\boldsymbol{\alpha}}.$$

Since $\boldsymbol{A} \in \partial\Phi(\dot{\boldsymbol{\alpha}})$, the definition (10) gives

$$\Phi(0) - \Phi(\dot{\boldsymbol{\alpha}}) \geqslant -\boldsymbol{A}.\dot{\boldsymbol{\alpha}}. \tag{13}$$

As noted above, Φ is positive and vanishes at 0. The left-hand side of (13) is thus non-positive, in compliance with the thermodynamical principle (8).

So far we have assumed that $\boldsymbol{\alpha}$ is *unconstrained*, in the sense that $\boldsymbol{\alpha}$ is allowed to take any value in $\mathbb{A}$. In order to model such phenomena as damage or phase-transformation, it is essential to consider an extension of (9) to situations where the internal variable $\boldsymbol{\alpha}$ is *constrained*, in the sense that $\boldsymbol{\alpha}$ is required to satisfy a condition of the form

$$\boldsymbol{\alpha} \in \mathcal{T}$$

where $\mathcal{T}$ is a given (usually bounded) convex subset of $\mathbb{A}$. In that case, as notably detailed by Frémond (2002), equations (9) are modified as

$$\begin{aligned} &\boldsymbol{\sigma} = \frac{\partial w}{\partial \boldsymbol{\varepsilon}}, \quad \boldsymbol{A} = -\frac{\partial w}{\partial \boldsymbol{\alpha}}, \quad s = -\frac{\partial w}{\partial \theta}, \\ &\boldsymbol{A} = \boldsymbol{A}^d + \boldsymbol{A}^r, \quad \boldsymbol{A}^d \in \partial\Phi(\dot{\boldsymbol{\alpha}}), \quad \boldsymbol{A}^r \in \partial I_{\mathcal{T}}(\boldsymbol{\alpha}) \end{aligned} \tag{14}$$

where $I_{\mathcal{T}}(\boldsymbol{\alpha})$ is the indicator function of $\mathcal{T}$ (equal to 0 if $\boldsymbol{\alpha} \in \mathcal{T}$, and infinite otherwise). The superscripts 'd' and 'r' in (14) stand for 'dissipative' and 'reversible', respectively.

Let us verify that the constitutive Eqs. (14) are consistent with the thermodynamic principles. From (14) we find

$$\boldsymbol{\sigma} : \dot{\boldsymbol{\varepsilon}} - s\dot{\theta} - \dot{w} = \boldsymbol{A}^d.\dot{\boldsymbol{\alpha}} + \boldsymbol{A}^r.\dot{\boldsymbol{\alpha}}. \tag{15}$$

The term $\boldsymbol{A}^d.\dot{\boldsymbol{\alpha}}$ can be proved to be positive using the same reasoning as in the unconstrained case. Since $\boldsymbol{\alpha}(t) \in \mathcal{T}$ for all t and $\boldsymbol{A}^r \in \partial I_{\mathcal{T}}(\boldsymbol{\alpha})$, the definition (10) implies that

$$I_{\mathcal{T}}(\boldsymbol{\alpha}(t - dt)) - I_{\mathcal{T}}(\boldsymbol{\alpha}(t)) \geqslant \boldsymbol{A}^r.(\boldsymbol{\alpha}(t - dt) - \boldsymbol{\alpha}(t)) \text{ for all } dt. \tag{16}$$

By letting dt tend towards 0 from above, we obtain that $\boldsymbol{A}^r.\dot{\boldsymbol{\alpha}} \geqslant 0$ where $\dot{\boldsymbol{\alpha}}$ is the left-time derivative. The left-hand side of (15) is thus positive, in accordance with (8). Note from (16) that if $\boldsymbol{\alpha}$ is time-differentiable (i.e. both left- and right-time derivatives exist and are equal), then $\boldsymbol{A}^r.\dot{\boldsymbol{\alpha}} = 0$. This remark will be useful in the next section. The property $\boldsymbol{A}^r.\dot{\boldsymbol{\alpha}} = 0$ also shows that $\boldsymbol{A}^r$ does not contribute to the energy dissipation, which explains why $\boldsymbol{A}^r$ is referred to as a 'reversible' term.

2.3. Boundary value problem

We now formulate the boundary value problem that governs quasi-static evolutions of a continuous medium submitted to a prescribed loading history. Body forces $\boldsymbol{f}^d$ are applied in the domain Ω. Displacements $\boldsymbol{u}^d$ are imposed on a part Γ_u of the boundary Γ, and tractions $\boldsymbol{T}^d$ are prescribed on $\Gamma_T = \Gamma - \Gamma_u$. The given functions $\boldsymbol{f}^d, \boldsymbol{u}^d, \boldsymbol{T}^d$ as well as the stress and state variables $(\boldsymbol{\sigma}, \boldsymbol{\varepsilon}, \boldsymbol{\alpha})$ in Ω, depend on the location $\boldsymbol{x}$ and the time t. However, in order to alleviate the expressions, this dependence will be omitted in the notations.

Combining the principle of virtual power (2) with the constitutive laws (14) leads to the following set of relations

$$\begin{aligned} &\boldsymbol{\sigma} \in \mathcal{K}_\sigma, \quad \boldsymbol{u} \in \mathcal{K}_u, \quad \boldsymbol{\alpha} \in \mathcal{K}_\alpha; \\ &\boldsymbol{\sigma} = \frac{\partial w}{\partial \boldsymbol{\varepsilon}}, \quad \boldsymbol{A} = -\frac{\partial w}{\partial \boldsymbol{\alpha}}, \quad s = -\frac{\partial w}{\partial \theta}; \\ &\boldsymbol{A} = \boldsymbol{A}^d + \boldsymbol{A}^r, \quad \boldsymbol{A}^d \in \partial\Phi(\dot{\boldsymbol{\alpha}}), \quad \boldsymbol{A}^r \in \partial I_{\mathcal{T}}(\boldsymbol{\alpha}); \end{aligned} \tag{17}$$

where the sets $\mathcal{K}_\sigma, \mathcal{K}_\epsilon, \mathcal{K}_\alpha$ are defined by

$$\begin{aligned} &\mathcal{K}_\sigma = \{\boldsymbol{\sigma} | \operatorname{div} \boldsymbol{\sigma} + \boldsymbol{f}^d = 0 \text{ in } \Omega; \boldsymbol{\sigma}.\boldsymbol{n} = \boldsymbol{T}^d \text{ on } \Gamma_T\}, \\ &\mathcal{K}_u = \{\boldsymbol{u} | \boldsymbol{u} = \boldsymbol{u}^d \text{ on } \Gamma_u\}, \\ &\mathcal{K}_\alpha = \{\boldsymbol{\alpha} | \boldsymbol{\alpha}(\boldsymbol{x}) \in \mathcal{T} \ \forall \boldsymbol{x} \text{ in } \Omega\}. \end{aligned}$$

In the isothermal case, the system (17) completely determines the evolution of the structure from a given initial state. It is important to note that the term $\boldsymbol{A}^r$ in (17) has a profound impact on the behaviour of the system compared to the classical plastic case. A more detailed discussion along those lines can be found in Peigney (2010).

Note that the free energy w depends on the temperature θ, so that the temperature appears implicitly in the last two equations of (17). In the coupled thermo-mechanical case, the temperature field $\theta(\boldsymbol{x}, t)$ is unknown and needs to be solved for. This is accomplished by using the energy balance Eq. (7) together with a constitutive law for heat conduction. In that regard, the most classical model of heat conduction is the Fourier's law $\boldsymbol{q} = -K\nabla\theta$, which we adopt in the following. To simplify the presentation, the (positive) thermal conductivity K is assumed to be independent on $\boldsymbol{x}$. Combining the energy balance (7) with Fourier's law yields the heat equation

$$K\Delta\theta - \theta\dot{s} + \boldsymbol{A}^d.\dot{\boldsymbol{\alpha}} + \boldsymbol{A}^r.\dot{\boldsymbol{\alpha}} + r = 0 \text{ a.e. in } \Omega \times [0, T]. \tag{18}$$

We assume in the following that $\boldsymbol{\alpha}(\boldsymbol{x}, t)$ is time-differentiable almost everywhere in $\Omega \times [0, T]$. As noted earlier, Eq. (16) then implies that $\boldsymbol{A}^r.\dot{\boldsymbol{\alpha}} = 0$ a.e. in $\Omega \times [0, T]$.

The Eq. (18) is complemented by thermal boundary conditions defined as follows: the temperature is prescribed to take a given value $\theta^d(\boldsymbol{x}, t)$ on a portion Γ_θ of the boundary $\partial\Omega$. The heat flux is prescribed to take a given value $q^d(\boldsymbol{x}, t)$ on a portion Γ_q such that $\Gamma_q \cap \Gamma_\theta = \emptyset$. On $\Gamma_h = \partial\Omega - \Gamma_\theta - \Gamma_q$, we consider a convection condition of the form

$$\boldsymbol{q}.\boldsymbol{n} = h(\theta - \theta_R) \tag{19}$$

where θ_R is the ambient temperature of the surrounding medium and h is a (positive) heat transfer coefficient. The temperature field θ is thus a solution of the boundary value problem

$$\begin{aligned} &\theta \in \mathcal{K}_\theta; \\ &-K\nabla\theta.\boldsymbol{n} = q^d \text{ on } \Gamma_q, \ -K\nabla\theta.\boldsymbol{n} = h(\theta - \theta_R) \text{ on } \Gamma_h; \\ &K\Delta\theta - \theta\dot{s} + \boldsymbol{A}^d.\dot{\boldsymbol{\alpha}} + r = 0 \text{ a.e. in } \Omega \times [0, T]; \end{aligned} \tag{20}$$

where $\mathcal{K}_\theta = \{\theta | \theta = \theta^d \text{ on } \Gamma_\theta\}$. The mechanical variables $(\boldsymbol{\alpha}, \boldsymbol{\varepsilon})$ have an influence on the solution θ of (20), both through the dependence of the entropy s on $(\boldsymbol{\alpha}, \boldsymbol{\varepsilon})$ and through the dissipative term $\boldsymbol{A}^d.\dot{\boldsymbol{\alpha}}$. In a similar fashion, as mentioned earlier, the solution of the mechanical problem (17) depends on the temperature field. The systems (17) and (20) are thus to be considered as *coupled*.

3. Variational formulation of an incremental problem

To solve a system such as (17)–(20), one generally resorts to a time-discretization strategy: the time history is discretized as a sequence $t_1 < t_2 < \cdots < t_n$ and one estimates successively the fields at time t_i using a finite time-step problem. That problem is an approximation of the time-continuous problem, allowing the fields $(\boldsymbol{\sigma}, \boldsymbol{u}, \boldsymbol{\alpha}, \theta)$ at $t^0 + \delta t$ (with $\delta t > 0$) to be estimated from their values $(\boldsymbol{\sigma}^0, \boldsymbol{u}^0, \boldsymbol{\alpha}^0, \theta^0)$ at t^0. Such a time-discretization scheme is required to be consistent with the rate problem, in the sense that the finite-step problem coincides with the rate problem (at least

formally) as the time increment δt tends towards 0. A second natural requirement is that the finite-step problem admits some solutions. In the isothermal case, such requirements are classically satisfied by the Euler implicit scheme. The corresponding finite-time step problem is

$$\begin{aligned}&\boldsymbol{\sigma}\in\mathcal{K}_\sigma,\quad \boldsymbol{u}\in\mathcal{K}_u,\quad \boldsymbol{\alpha}\in\mathcal{K}_\alpha;\\&\boldsymbol{\sigma}=\frac{\partial w}{\partial\boldsymbol{\varepsilon}},\boldsymbol{A}=-\frac{\partial w}{\partial\boldsymbol{\alpha}};\\&\boldsymbol{A}=\boldsymbol{A}^d+\boldsymbol{A}^r,\quad \boldsymbol{A}^d\in\partial\Phi\left(\frac{\boldsymbol{\alpha}-\boldsymbol{\alpha}^0}{\delta t}\right),\quad \boldsymbol{A}^r\in\partial I_{\mathcal{T}}(\boldsymbol{\alpha}).\end{aligned}\tag{21}$$

The incremental problem (21) can easily be verified to be consistent with the rate problem (17). Existence of solutions can be studied by using a variational formulation attached to (21). To that purpose, introduce the functionals $\mathcal{F}^e$ and $\mathcal{F}_0^d$ defined as

$$\begin{aligned}&\mathcal{F}^e(\boldsymbol{u},\boldsymbol{\alpha},\theta)=\int_\Omega w(\boldsymbol{\varepsilon},\boldsymbol{\alpha},\theta)d\omega-\int_\Omega \boldsymbol{f}^d.\boldsymbol{u}\,d\omega-\int_{\Gamma_T}\boldsymbol{T}^d.\boldsymbol{u}\,da;\\&\mathcal{F}_0^d(\boldsymbol{\alpha})=\int_\Omega\Phi(\boldsymbol{\alpha}-\boldsymbol{\alpha}^0)d\omega.\end{aligned}\tag{22}$$

The functional $\mathcal{F}^e$ is the potential elastic energy of the system, while $\mathcal{F}_0^d$ is related to the energy dissipated on the time interval $[t^0,t^0+\delta t]$.

The functional $\mathcal{F}_0=\mathcal{F}^e+\mathcal{F}_0^d$ is differentiable with respect to $\boldsymbol{u}$ but only subdifferentiable with respect to $\boldsymbol{\alpha}$. The derivative of $\mathcal{F}_0$ with respect to $\boldsymbol{u}$ is denoted by $\partial\mathcal{F}_0/\partial u$. The subdifferential of $\mathcal{F}_0$ is denoted by $\partial_\alpha\mathcal{F}_0$ and is characterized as follows: for any $\mathcal{A}\in\partial_\alpha\mathcal{F}_0(\boldsymbol{u},\boldsymbol{\alpha},\theta)$, there exists a field $\boldsymbol{A}^d$ such that $\boldsymbol{A}^d\in\partial\Phi(\boldsymbol{\alpha}-\boldsymbol{\alpha}^0)$ and

$$\mathcal{A}.(\boldsymbol{\alpha}^*-\boldsymbol{\alpha})=\int_\Omega\left(\frac{\partial w}{\partial\boldsymbol{\alpha}}+\boldsymbol{A}^d\right).(\boldsymbol{\alpha}^*-\boldsymbol{\alpha})d\omega\ \forall\boldsymbol{\alpha}^*\in\mathcal{K}_\alpha.$$

We note that $\mathcal{A}.(\boldsymbol{\alpha}^*-\boldsymbol{\alpha})$ can be interpreted as the directional derivative of $\mathcal{F}_0$ in the direction $\boldsymbol{\alpha}^*-\boldsymbol{\alpha}$ (Rockafellar, 1970).

The introduction of the functional $\mathcal{F}_0$ is motivated by the following property: any solution of (21) is a solution of the variational problem

$$\begin{aligned}&\textit{Find }(\boldsymbol{u},\boldsymbol{\alpha})\in\mathcal{K}_u\times\mathcal{K}_\alpha\textit{ and }\mathcal{A}\in\partial_\alpha\mathcal{F}_0(\boldsymbol{u},\boldsymbol{\alpha},\theta)\textit{ such that}:\\&0\leqslant\frac{\partial\mathcal{F}_0}{\partial\boldsymbol{u}}.(\boldsymbol{u}^*-\boldsymbol{u})+\mathcal{A}.(\boldsymbol{\alpha}^*-\boldsymbol{\alpha})\quad\forall(\boldsymbol{u}^*,\boldsymbol{\alpha}^*)\in\mathcal{K}_u\times\mathcal{K}_\alpha.\end{aligned}\tag{23}$$

Let us justify that statement. The stationarity conditions with respect to $\boldsymbol{u}$ in (23) give the equations $\boldsymbol{\sigma}=\partial w/\partial\boldsymbol{\varepsilon}$ and $\boldsymbol{\sigma}\in\mathcal{K}_\sigma$. The stationarity conditions with respect to $\boldsymbol{\alpha}$ give

$$-\boldsymbol{A}.(\boldsymbol{\alpha}^*-\boldsymbol{\alpha})+\boldsymbol{A}^d.(\boldsymbol{\alpha}^*-\boldsymbol{\alpha})\geqslant 0\ \forall\boldsymbol{\alpha}^*\in\mathcal{T};\tag{24}$$

where $\boldsymbol{A}=-\partial w/\partial\boldsymbol{\alpha}$ and $\boldsymbol{A}^d\in\partial\Phi(\boldsymbol{\alpha}-\boldsymbol{\alpha}^0)$. The Eq. (24) implies that $\boldsymbol{A}-\boldsymbol{A}^d\in\partial I_{\mathcal{T}}(\boldsymbol{\alpha})$, i.e. there exists $\boldsymbol{A}^r\in\partial I_{\mathcal{T}}(\boldsymbol{\alpha})$ such that $\boldsymbol{A}=\boldsymbol{A}^d+\boldsymbol{A}^r$. □

The variational formulation (23) means that the directional derivative of $\mathcal{F}_0$ in every direction is positive. Such a condition is notably satisfied if $\mathcal{F}_0$ reaches a local minimum at $(\boldsymbol{u},\boldsymbol{\alpha})$. In the particular case where $\mathcal{F}_0$ is convex, it is known that local minima coincide with global minima, and are the only solutions of the problem (23). In such condition, the problem (23) is equivalent to

$$\min_{(\boldsymbol{u},\boldsymbol{\alpha})\in\mathcal{K}_u\times\mathcal{K}_\alpha}\mathcal{F}^e(\boldsymbol{u},\boldsymbol{\alpha},\theta)+\mathcal{F}_0^d(\boldsymbol{\alpha})\tag{25}$$

and admits solutions in adequate functional spaces for $\mathcal{K}_u$ and $\mathcal{K}_\alpha$. This in turn ensures the existence of solutions to the isothermal incremental problem (21).

Note that the functional $\mathcal{F}_0^d$ is convex. A sufficient condition for $\mathcal{F}_0$ to be convex is thus that the free energy w is convex in $(\boldsymbol{\varepsilon},\boldsymbol{\alpha})$, which is notably satisfied by a wide range of elastoplasticity models. We note, however, that the requirement of convexity on w is not mandatory for (25) to have a solution. For instance, arguments related to quasiconvexity can be used to study the existence of solution to (25) in a more general setting (see e.g. Dacorogna, 2008).

Let us give some interpretation of (25). When there is no dissipation, it is well known that the solutions of the equilibrium problem minimize the potential elastic energy $\mathcal{F}^e$. The relation (25) can be interpreted as an extension of the principle of energy minimization to dissipative evolutions: the state of the system at time $t^0+\delta t$ is obtained by minimizing the 'incremental energy' $\mathcal{F}_0$. In the expression of $\mathcal{F}_0$, the dissipative contribution $\mathcal{F}_0^d$ depends on the state $\boldsymbol{\alpha}^0$ of the system at time t^0. Therefore, the state of the system at time $t^0+\delta t$ also depends on $\boldsymbol{\alpha}^0$, which reflects the path-dependence of dissipative evolutions.

We now move to the coupled thermo-mechanical problem (17)–(20). A natural choice is to use again the Euler implicit scheme, which now reads:

$$\boldsymbol{\sigma}\in\mathcal{K}_\sigma,\quad \boldsymbol{u}\in\mathcal{K}_u,\quad \boldsymbol{\alpha}\in\mathcal{K}_\alpha,\quad \theta\in\mathcal{K}_\theta;\tag{26.1}$$

$$\boldsymbol{\sigma}=\frac{\partial w}{\partial\boldsymbol{\varepsilon}},\quad \boldsymbol{A}=-\frac{\partial w}{\partial\boldsymbol{\alpha}},\quad s=-\frac{\partial w}{\partial\theta};\tag{26.2}$$

$$\boldsymbol{A}=\boldsymbol{A}^r+\boldsymbol{A}^d,\quad \boldsymbol{A}^r\in\partial I_{\mathcal{T}}(\boldsymbol{\alpha}),\quad \boldsymbol{A}^d\in\partial\Phi\big((\boldsymbol{\alpha}-\boldsymbol{\alpha}^0)/\delta t\big);\tag{26.3}$$

$$-K\nabla\theta.\boldsymbol{n}=q^d\text{ on }\Gamma_q,\quad -K\nabla\theta.\boldsymbol{n}=h(\theta-\theta_R)\text{ on }\Gamma_h;\tag{26.4}$$

$$K\delta t\Delta\theta-\theta^0(s-s^0)+\boldsymbol{A}^d.(\boldsymbol{\alpha}-\boldsymbol{\alpha}^0)+r\delta t=0;\tag{26.5}$$

where $s^0=s(\boldsymbol{\varepsilon}^0,\boldsymbol{\alpha}^0,\theta^0)$. That incremental problem is obviously consistent with the rate problem. In particular, dividing (26.5) by δt and taking the limit $\delta t\to 0$ yields the rate form of the heat equation in (20). However, existence of solutions to (26) cannot be proved in general. This is essentially due to the lack of a variational formulation for (26): in contrast with the isothermal problem (21), the incremental problem (26) does not correspond to the stationarity conditions of a certain functional.

In order to avoid such difficulties, consider instead the following finite time-step problem:

$$\boldsymbol{\sigma}\in\mathcal{K}_\sigma,\quad \boldsymbol{u}\in\mathcal{K}_u,\quad \boldsymbol{\alpha}\in\mathcal{K}_\alpha,\quad \theta\in\mathcal{K}_\theta;\tag{27.1}$$

$$\boldsymbol{\sigma}=\frac{\partial w}{\partial\boldsymbol{\varepsilon}},\quad \boldsymbol{A}=-\frac{\partial w}{\partial\boldsymbol{\alpha}},\quad s=-\frac{\partial w}{\partial\theta};\tag{27.2}$$

$$\boldsymbol{A}=\boldsymbol{A}^r+\frac{\theta}{\theta^0}\boldsymbol{A}^d,\quad \boldsymbol{A}^r\in\partial I_{\mathcal{T}}(\boldsymbol{\alpha}),\quad \boldsymbol{A}^d\in\partial\Phi\big((\boldsymbol{\alpha}-\boldsymbol{\alpha}^0)/\delta t\big);\tag{27.3}$$

$$-K\nabla\theta.\boldsymbol{n}=q^d\text{ on }\Gamma_q,\quad -K\nabla\theta.\boldsymbol{n}=h(\theta-\theta_R)\text{ on }\Gamma_h;\tag{27.4}$$

$$K\delta t\left[\Delta\theta+\frac{\nabla\theta^0}{\theta^0}.\nabla(\theta^0-\theta)\right]-\theta^0(s-s^0)+\boldsymbol{A}^d.(\boldsymbol{\alpha}-\boldsymbol{\alpha}^0)+r\delta t=0.\tag{27.5}$$

That problem differs from (26) in two points: a factor θ/θ^0 is added in (27.3), and a term $K\delta t\nabla\theta^0.\nabla(\theta^0-\theta)/\theta^0$ is added in the heat equation (27.5). It can be verified that – just as the more intuitive scheme (26) – the incremental problem (27) is a consistent time-discretization of (17)–(20). In particular, the heat equation in (20) is again recovered by dividing 27.5 by δt and taking the limit $\delta t\to 0$. The crucial point here is that the extra term $K\delta t\nabla\theta^0.\nabla(\theta^0-\theta)/\theta^0$ is of the second order in δt.

Motivation of the scheme (27) is that a variational formulation can be given. The corresponding functional is an extension of (22) to thermo-mechanics, and is given by

$$\mathcal{F}(\boldsymbol{u},\boldsymbol{\alpha},\theta)=\mathcal{F}^e(\boldsymbol{u},\boldsymbol{\alpha},\theta)+\mathcal{F}^d(\boldsymbol{\alpha},\theta)+\mathcal{F}^\theta(\theta)$$

where

$$\mathcal{F}^d(\boldsymbol{\alpha},\theta)=\int_\Omega \frac{\theta}{\theta^0}\Phi(\boldsymbol{\alpha}-\boldsymbol{\alpha}^0)\,d\omega;$$

$$\mathcal{F}^\theta(\theta)=\int_\Omega \theta\left(s^0+\delta t\frac{r}{\theta^0}\right)d\omega + \delta t\int_\Omega K\left(-\frac{1}{2}\frac{1}{\theta^0}\|\nabla\theta\|^2+\left(\frac{\|\nabla\theta^0\|}{\theta^0}\right)^2\theta\right)d\omega - \delta t\int_{\Gamma_q}\frac{q^d}{\theta^0}\theta\,da-h\frac{\delta t}{2}\int_{\Gamma_h}\frac{(\theta-\theta_R)^2}{\theta^0}da. \quad (28)$$

Note that $\mathcal{F}^\theta$ is a quadratic and concave function of θ. In a way similar to the isothermal case, the functional $\mathcal{F}$ is differentiable with respect to $\boldsymbol{u}$ and θ (with partial derivatives denoted by $\partial\mathcal{F}/\partial\boldsymbol{u}$ and $\partial\mathcal{F}/\partial\theta$) and only subdifferentiable with respect to $\boldsymbol{\alpha}$. The subdifferential of $\mathcal{F}$ with respect to $\boldsymbol{\alpha}$ is the multivalued mapping characterized as follows: for any $\mathcal{A}\in\partial_{\boldsymbol{\alpha}}\mathcal{F}(\boldsymbol{u},\boldsymbol{\alpha},\theta)$, there exists a field $\boldsymbol{A}^d$ such that $\boldsymbol{A}^d\in\partial\Phi(\boldsymbol{\alpha}-\boldsymbol{\alpha}^0)$ and

$$\mathcal{A}.(\boldsymbol{\alpha}^*-\boldsymbol{\alpha})=\int_\Omega\left(\frac{\partial w}{\partial\boldsymbol{\alpha}}+\frac{\theta}{\theta^0}\boldsymbol{A}^d\right).(\boldsymbol{\alpha}^*-\boldsymbol{\alpha})d\omega\ \forall\boldsymbol{\alpha}^*\in\mathcal{K}_\alpha.$$

As detailed in Appendix A, any solution of (27) is a solution of the following variational problem

Find $(\boldsymbol{u},\boldsymbol{\alpha},\theta)\in\mathcal{K}_u\times\mathcal{K}_\alpha\times\mathcal{K}_\theta$ *and* $\mathcal{A}\in\partial_{\boldsymbol{\alpha}}\mathcal{F}(\boldsymbol{u},\boldsymbol{\alpha},\theta)$ *such that*

$$0\leqslant\frac{\partial\mathcal{F}}{\partial\boldsymbol{u}}.(\boldsymbol{u}^*-\boldsymbol{u})+\frac{\partial\mathcal{F}}{\partial\theta}.(\theta^*-\theta)+\mathcal{A}.(\boldsymbol{\alpha}^*-\boldsymbol{\alpha})\ \forall(\boldsymbol{u}^*,\boldsymbol{\alpha}^*,\theta^*)\in\mathcal{K}_u\times\mathcal{K}_\alpha\times\mathcal{K}_\theta. \quad (29)$$

As in the isothermal case, the variational formulation (29) allows the existence of solutions to (27) to be studied. Assume in particular that the free energy w is convex in $(\boldsymbol{u},\boldsymbol{\alpha})$ and concave in θ. In such a situation, the functional $\mathcal{F}$ is convex with respect to the fields $(\boldsymbol{u},\boldsymbol{\alpha})$ and concave with respect to θ, so that a saddle point exists (in adequate functional spaces for $\mathcal{K}_u,\mathcal{K}_\alpha$ and $\mathcal{K}_\theta$, depending on the growth behaviour of w and Φ at infinity). Such a saddle point $(\boldsymbol{u},\boldsymbol{\alpha},\theta)$ verifies (29) and therefore is a solution of the incremental problem (27).

The incremental thermo-mechanical problem (27) is an extension of an incremental problem introduced in Peigney (2006) for a simplified thermo-mechanical setting (in which the dissipative contribution $\boldsymbol{A}^d.\dot{\boldsymbol{\alpha}}$ is neglected in the heat Eq. (20)).

4. A maximization approach for solving the incremental problem

To solve a problem such as (26) or (27), a general strategy is to directly solve the local equations using for instance a Newton–Raphson algorithm. In such a framework, a partitioning approach is often used: the mechanical and the thermal subproblems are decoupled and solved successively until convergence, as described in Algorithm 1 below (see e.g. Auricchio and Petrini, 2004 for an example of that approach). The global convergence of such methods is not ensured, and in practice one can face difficulties of convergence notably when the initial guess is not close enough to the solution.

Algorithm 1. Partitioning method for the thermo-mechanical problem (26)

$k\leftarrow 0$
while *residual* > *tolerance* **do**
  Compute $(\boldsymbol{u}^{k+1},\boldsymbol{\alpha}^{k+1})$ as the solution of (26.1)–(26.3) at $\theta=\theta^k$
  Compute θ^{k+1} as the solution of (26.4),(26.5) at $(\boldsymbol{u},\boldsymbol{\alpha})=(\boldsymbol{u}^{k+1},\boldsymbol{\alpha}^{k+1})$
  $k\leftarrow k+1$
end while

Observe that, in the case of (27), such strategies ignore the variational nature of the problem at hand. As an alternative, using the variational formulation of the problem, the solution of (27) can be found by solving a concave maximization problem, as detailed in the following. We assume that w is convex in $(\boldsymbol{u},\boldsymbol{\alpha})$ and concave in θ, which ensures that (27) has a solution. More precisely, as explained at the end of Section 3, solutions of (27) are saddle points of $\mathcal{F}$, i.e solutions of the max–min problem

$$\max_{\theta\in\mathcal{K}_\theta}\min_{(\boldsymbol{u},\boldsymbol{\alpha})\in\mathcal{K}_u\times\mathcal{K}_\alpha}\mathcal{F}^e(\boldsymbol{u},\boldsymbol{\alpha},\theta)+\mathcal{F}^d(\boldsymbol{\alpha},\theta)+\mathcal{F}^\theta(\theta). \quad (30)$$

The problem (30) can be rewritten as

$$\max_{\theta\in\mathcal{K}_\theta}J(\theta) \quad (31)$$

where the functional J is defined as

$$J(\theta)=\mathcal{F}^\theta(\theta)+\min_{(\boldsymbol{u},\boldsymbol{\alpha})\in\mathcal{K}_u\times\mathcal{K}_\alpha}\{\mathcal{F}^e(\boldsymbol{u},\boldsymbol{\alpha},\theta)+\mathcal{F}^d(\boldsymbol{\alpha},\theta)\} \quad (32)$$

and can be proved to be concave (see Appendix B).

Solving the set of partial differential equations (27) amounts to solve the concave maximization problem (31) with respect to the temperature field. A lot of well-known algorithms can be used to solve such a maximization problem, some of them being built-in functions of scientific calculation softwares. Such algorithms (like the Broyden–Fletcher–Goldfarb–Shanno algorithm for instance) are iterative and typically require the computation of J and its gradient J' (or at least of an ascent direction) at each iteration. In this regard, note from (32) that the calculation of $J(\theta)$ amounts to solve the minimization problem

$$\min_{(\boldsymbol{u},\boldsymbol{\alpha})\in\mathcal{K}_u\times\mathcal{K}_\alpha}\mathcal{F}^e(\boldsymbol{u},\boldsymbol{\alpha},\theta)+\mathcal{F}^d(\boldsymbol{\alpha},\theta) \quad (33)$$

for which the local equations (expressing the stationarity of the functional) read as

$$\boldsymbol{u}\in\mathcal{K}_u,\boldsymbol{\sigma}\in\mathcal{K}_\sigma,\quad \boldsymbol{\alpha}\in\mathcal{K}_\alpha;$$
$$\boldsymbol{\sigma}=\frac{\partial w}{\partial\boldsymbol{\varepsilon}},\quad \boldsymbol{A}=-\frac{\partial w}{\partial\boldsymbol{\alpha}};$$
$$\boldsymbol{A}=\boldsymbol{A}^d+\boldsymbol{A}^r,\quad \boldsymbol{A}^d\in\frac{\theta}{\theta^0}\partial\Phi\left(\frac{\boldsymbol{\alpha}-\boldsymbol{\alpha}^0}{\delta t}\right),\quad \boldsymbol{A}^r\in\partial I_{\mathcal{T}}(\boldsymbol{\alpha}). \quad (34)$$

That problem is formally identical to the isothermal problem (21), with a dissipation potential set equal to $(\theta/\theta_0)\Phi$. The calculation of $J(\theta)$ thus amounts to solve a incremental problem at a fixed temperature field.

Special care must be taken in the calculation of $J'(\theta)$ because, due to the non-differentiable nature of Φ, it is not ensured that J is differentiable everywhere. However, since J is concave, there exists a directional derivative in every direction (Rockafellar, 1970). For a given $\theta\in\mathcal{K}_\theta$ and $\tilde{\theta}$ such that $\tilde{\theta}=0$ on Γ_θ, the directional derivative $DJ(\theta;\tilde{\theta})$ at θ in direction $\tilde{\theta}$ is defined by

$$DJ(\theta;\tilde{\theta})=\lim_{t\longrightarrow 0^+}\frac{J(\theta(t))-J(\theta)}{t}$$

where $\theta(t)=\theta+t\tilde{\theta}\in\mathcal{K}_\theta$. As detailed in Appendix B, the directional derivative of J satisfies the property

$$DJ(\theta,\tilde{\theta})\geqslant\frac{\partial\mathcal{F}}{\partial\theta}.\tilde{\theta} \quad (35)$$

with

$$\frac{\partial\mathcal{F}}{\partial\theta}.\tilde{\theta}=\int_\Omega\left[\theta^0(s^0-s)+r\delta t+\boldsymbol{A}^d.(\boldsymbol{\alpha}-\boldsymbol{\alpha}^0)+K\delta t\left(\frac{\|\nabla\theta^0\|^2}{\theta^0}-\frac{\nabla\theta.\nabla\theta^0}{\theta^0}+\Delta\theta\right)\right]\frac{\tilde{\theta}}{\theta^0}d\omega - \delta t\int_{\Gamma_q}\frac{q^d+K\nabla\theta.n}{\theta^0}\tilde{\theta}\,da-\delta t\int_{\Gamma_h}\frac{h(\theta-\theta_R)+K\nabla\theta.n}{\theta^0}\tilde{\theta}\,da. \quad (36)$$

In order to determine an ascent direction for J, consider the solution W of the following linear problem:

$$\begin{aligned}
&\Delta W - W = -\frac{1}{\theta^0}\left[K\delta t(\Delta\theta) + \frac{\nabla\theta^0}{\theta^0}.\nabla(\theta^0-\theta) - \theta^0(s-s^0) + \boldsymbol{A}^d.(\boldsymbol{\alpha}-\boldsymbol{\alpha}^0) + r\delta t\right];\\
&W = 0 \text{ on } \Gamma_\theta;\\
&\nabla W.\boldsymbol{n} = \frac{\delta t}{\theta^0}(K\nabla\theta.\boldsymbol{n} + q^d) \text{ on } \Gamma_q;\\
&\nabla W.\boldsymbol{n} = \frac{\delta t}{\theta^0}(K\nabla\theta.\boldsymbol{n} + h(\theta-\theta_R)) \text{ on } \Gamma_h.
\end{aligned} \tag{37}$$

Substituting in the expression (36) gives

$$\begin{aligned}
\frac{\partial\mathcal{F}}{\partial\theta}.\tilde{\theta} &= \int_\Omega(-\Delta W + W)\tilde{\theta}d\omega - \int_{\partial\Omega}\tilde{\theta}\nabla W.\boldsymbol{n}da\\
&= \int_\Omega(\nabla W.\nabla\tilde{\theta} + W\tilde{\theta})d\omega.
\end{aligned}$$

The relation (35) then implies that

$$DJ(\theta;\tilde{\theta}) \geqslant \int_\Omega(\nabla W.\nabla\tilde{\theta} + W\tilde{\theta})d\omega.$$

In particular, we have $DJ(\theta;W) = \int_\Omega(W^2 + \|\nabla W\|^2) \geqslant 0$, i.e. W is an ascent direction for J. Note that $DJ(\theta;W)$ is null if and only if θ is solution of the maximization problem (31). The introduction of an auxiliary problem for determining an ascent direction is reminiscent of techniques used in optimal control theory (Lions, 1968). That theory addresses minimization problems of the form $\min_a J(s(a))$ in which $s(a)$ is solution of a set of partial differential equations parametrized by a. In the optimal control terminology, a is the *control variable* and $s(a)$ is the *state variable*. In general, the set of partial differential equations that defines $s(a)$ cannot be solved in closed-form, so that the dependence of J with respect to a remains implicit. The explicit determination of the gradient J' is thus not straightforward. An effective method is to introduce a so-called *adjoint state* for expressing J'. That adjoint state is usually defined as the solution of an ad hoc set of linear partial differential equations. In solid mechanics, the optimal control theory has been extensively used for inverse problems (Bui, 2006) and also proved to be useful for other classes of nonlinear problems (Peigney and Stolz, 2001; Peigney and Stolz, 2003; Stolz, 2008). Note that the maximization problem (31) can be interpreted as an optimal control problem, the temperature field θ being the control variable and the mechanical fields $(\boldsymbol{u},\boldsymbol{\alpha})$ being the state variable. The fields $(\boldsymbol{u},\boldsymbol{\alpha})$ are indeed solution of the set of partial differential Eqs. (34) in which θ acts as an external parameter. The field W defined in (37) can be interpreted as the adjoint state for that problem.

Algorithm 2. Maximization method for the thermo-mechanical problem (27).

$k \leftarrow 0$
while *residual* > *tolerance* **do**
  Compute $J(\theta^k)$ by solving (34) at $\theta = \theta^k$
  Compute W^k as the solution of (37)
  $\theta^{k+1} = \theta^k +$ ascent $(J(\theta^k), W^k)$
  $k \leftarrow k+1$
end while

Collecting the results obtained leads to Algorithm 2 for solving the incremental thermo-mechanical problem (27). At each iteration, a mechanical problem at a fixed temperature field is solved for evaluating J, and a scalar problem is solved for determining an ascent direction W^k. The results are used to feed an ascent algorithm for updating the temperature field. One of the simplest choices consists in performing a line search in the direction W^k.

Algorithm 2 retains some attractive features of Algorithm 1, such as the decoupling between mechanical and thermal subproblems. The mechanical subproblems in both those algorithms have the same structure. In contrast, the thermal subproblem (37) in Algorithm 2 is linear, whereas the thermal problem (26.4),(26.5) in Algorithm 1 generally is not. The proposed method has the advantage of relying on a sound mathematical framework, which bodes well for robustness and convergence properties.

5. Application to shape-memory alloys

The formulation derived so far is now applied to shape memory alloys. Such material indeed exhibit strong thermo-mechanical coupling (notably through latent heat effects) and therefore offer a relevant application for illustrating the proposed method. It is not the purpose of this paper to give a detailed presentation of shape-memory alloys (see e.g. the books by Otsuka and Wayman (1999) and Bhattacharya et al. (2003)). We simply mention that the peculiar properties of those materials stem from a solid/solid phase transformation between different crystallographic structures, known as austenite and martensite. The martensitic lattice has less symmetry than the austenitic one, which leads one to distinguish several martensitic variants, identified as individual phases.

Here we consider a micromechanical model of shape-memory alloys, for which the internal variable $\boldsymbol{\alpha} = (\alpha_1,\ldots,\alpha_n)$ corresponds to the volume fractions of the n martensitic variants. Because of mass conservation in the phase-transformation process, the variable $\boldsymbol{\alpha}$ must belong to the n-dimensional tetrahedron $\mathcal{T}$ defined as

$$\mathcal{T} = \left\{\boldsymbol{\alpha}\in\mathbb{R}^n | \alpha_i \geqslant 0 \ \forall i; \sum_{i=1}^n \alpha_i \leqslant 1\right\}. \tag{38}$$

We consider a Helmholtz free energy w and a dissipation potential Φ given by the following expressions (Abeyaratne et al., 1994; Govindjee and Miehe, 2001; Anand and Gurtin, 2003):

$$\begin{aligned}
w(\boldsymbol{\varepsilon},\boldsymbol{\alpha},\theta) = \frac{1}{2}&\left(\boldsymbol{\varepsilon} - \sum_{i=1}^n \alpha_i\boldsymbol{\varepsilon}_i^{tr}\right) : \boldsymbol{L}\\
&: \left(\boldsymbol{\varepsilon} - \sum_{i=1}^n \alpha_i\boldsymbol{\varepsilon}_i^{tr}\right) + \frac{\lambda_T}{\theta_T}(\theta-\theta_T)\sum_{i=1}^n\alpha_i\\
&+ c\left(\theta - \theta_R - \theta\log\left(\frac{\theta}{\theta_R}\right)\right),
\end{aligned} \tag{39}$$

$$\Phi(\dot{\boldsymbol{\alpha}}) = \boldsymbol{G}^+.\langle\dot{\boldsymbol{\alpha}}\rangle_+ + \boldsymbol{G}^-.\langle\dot{\boldsymbol{\alpha}}\rangle_-. \tag{40}$$

where $\langle\boldsymbol{x}\rangle_+$ denotes the positive vector whose component i is $\max(0,x_i)$. Similarly, for any vector $\boldsymbol{x}$, $\langle\boldsymbol{x}\rangle_-$ is the positive vector with components $\max(0,-x_i)$. In (40), $\boldsymbol{G}^+$ and $\boldsymbol{G}^-$ are two given positive vectors of $\mathbb{R}^n$ that characterize the mechanical dissipation in the model. In (39), the so-called transformation strains $\boldsymbol{\varepsilon}_i^{tr}$ are obtained from the crystallographic structure of the alloy considered. The elasticity tensor $\boldsymbol{L}$ is symmetric positive definite. The parameter λ_T is the latent heat at the transformation temperature θ_T, and c is the specific heat. We refer to Govindjee and Miehe (2001), Hackl and Heinen (2008), Peigney (2009), Peigney (2013a) and Peigney (2013b) for more details and recent developments on micromechanical modelling of shape-memory alloys.

As detailed in Section 4, solving the thermo-mechanical problem (31) partly relies on solving the isothermal problem (21). For the material model considered here, the isothermal problem (21) specializes as

$$\begin{aligned}
&\boldsymbol{\sigma} \in \mathcal{K}_\sigma, \quad \boldsymbol{u} \in \mathcal{K}_u, \quad \boldsymbol{\alpha} \in \mathcal{K}_\alpha;\\
&\boldsymbol{\sigma} = \boldsymbol{L} : \left(\boldsymbol{\varepsilon} - \sum_{i=1}^{n} \alpha_i \boldsymbol{\varepsilon}_i^{tr}\right);\\
&\boldsymbol{A} = (\boldsymbol{\varepsilon}_1^{tr} : \boldsymbol{\sigma}, \ldots, \boldsymbol{\varepsilon}_n^{tr} : \boldsymbol{\sigma});\\
&\boldsymbol{A} = \boldsymbol{A}^d + \boldsymbol{A}^r, \quad \boldsymbol{A}^d \in \partial\Phi\left(\frac{\boldsymbol{\alpha} - \boldsymbol{\alpha}^0}{\delta t}\right), \quad \boldsymbol{A}^r \in \partial I_{\mathcal{T}}(\boldsymbol{\alpha});
\end{aligned} \tag{41}$$

where the subdifferentials $\partial\Phi$ and $\partial I_{\mathcal{T}}$ are characterized as follows:

$$\boldsymbol{A}^d = (A_1^d, \ldots, A_n^d) \in \partial\Phi\left(\frac{\boldsymbol{\alpha} - \boldsymbol{\alpha}^0}{\delta t}\right) \Longleftrightarrow \begin{cases} A_i^d = G_i^+ & \text{if } \alpha_i > \alpha_0^i \\ = -G_i^- & \text{if } \alpha_i < \alpha_0^i \\ \in [-G_i^-, G_i^+] & \text{if } \alpha_i = \alpha_0^i \end{cases}$$

and

$$\boldsymbol{A}^r = (A_1^r, \ldots, A_n^r) \in \partial I_{\mathcal{T}}(\boldsymbol{\alpha}) \Longleftrightarrow \begin{array}{l} \text{there exists } z \in \mathbb{R}_+ \text{ and } a_i \in \mathbb{R}_+ \text{ such that} \\ A_i^r = z - a_i;\ z\left(1 - \sum_{i=1}^{n} \alpha_i\right);\ \ \alpha_i a_i = 0. \end{array}$$

Concerning the thermal equations, note from (39) that the entropy s is given by

$$s = -\frac{\lambda_T}{\theta_T} \sum_{i=1}^{n} \alpha_i + c \log\left(\frac{\theta}{\theta_R}\right)$$

so that the heat Eq. (20) becomes

$$c\dot{\theta} - K\Delta\theta = \lambda_T \frac{\theta}{\theta_T}\left(\sum_{i=1}^{n} \dot{\alpha}_i\right) + [\boldsymbol{G}^+ . \langle \dot{\boldsymbol{\alpha}} \rangle_+ + \boldsymbol{G}^- . \langle \dot{\boldsymbol{\alpha}} \rangle_-] + r. \tag{42}$$

Apart from the external heat source r, the two terms on the right-hand side can be interpreted as internal heat sources due to phase transformation. They are respectively associated with the latent heat (reversible contribution) and with the mechanical dissipation (irreversible contribution). Depending on the rate of loading and on the thermal exchange conditions, the heat produced by the phase transformation may not have time to diffuse in the body and the temperature field may become inhomogeneous. In such conditions, the overall stress–strain response becomes significantly different from its isothermal counterpart. Such effects are explored in more detail in the following.

5.1. Influence of the strain rate

The first example we consider is inspired by the experiments of Shield (1995). We consider a monocrystalline CuAlNi strip with dimensions 38 mm × 6 mm × 1 mm, submitted to displacement-controlled traction along the x-axis (Fig. 1). The end section at $x = 0$ is clamped. On the end section at $x = L$ (L =38 mm), the displacements along the $\boldsymbol{e}_z$ and $\boldsymbol{e}_y$ axes are set equal to 0 and the displacement $u^*(t)$ along the $\boldsymbol{e}_x$ axis is prescribed as

$$u^*(t) = \begin{cases} \frac{t}{T} u^*_{max} & \text{for } 0 \leqslant t \leqslant T \\ (2 - \frac{t}{T}) u^*_{max} & \text{for } T \leqslant t \leqslant 2T \end{cases} \tag{43}$$

where u^*_{max} and T are fixed. The loading strain rate $\dot{\varepsilon}^*$ is defined as

$$\dot{\varepsilon}^* = \left|\frac{d}{dt}\left(\frac{u^*}{L}\right)\right| = \frac{u^*_{max}}{LT}.$$

A null heat flux is prescribed on both end sections of the sample. A convection boundary condition of the form (19) is assumed on the lateral surface S_{lat}. We consider two different thermal boundary conditions on the end sections, labeled as (i) and (ii). Boundary condition (i) consists in imposing a null heat flux on the end sections $x \in \{0, L\}$. Boundary condition (ii) consists in imposing $\theta = \theta_R$ on the two end sections. Those two boundary conditions can be interpreted as limiting cases of the convection condition (19), with $h = 0$ and $h = \infty$, respectively.

In the initial state, the structure is fully austenitic (i.e. $\boldsymbol{\alpha}(\boldsymbol{x}, 0) = 0$ for all $\boldsymbol{x}$) and in thermal equilibrium (i.e. $\theta(\boldsymbol{x}, 0) = \theta_R$).

There are six martensitic variants in CuAlNi (Otsuka and Wayman, 1999; Bhattacharya, 1993). The six transformation strains $\boldsymbol{\varepsilon}_i^{tr}$, expressed in the (x, y, z) basis of Fig. 1, take the form

$$\boldsymbol{\varepsilon}_i^{tr} = \boldsymbol{R}^T . \boldsymbol{\varepsilon}_{0,i}^{tr} . \boldsymbol{R}$$

where $\boldsymbol{\varepsilon}_{0,i}^{tr}$ ($i = 1, \ldots, 6$) are the reference transformation strains (expressed in the natural basis of the austenitic cubic lattice) and $\boldsymbol{R}$ is a rotation describing the orientation of the sample with respect to the austenitic lattice. The reference transformation strains $\boldsymbol{\varepsilon}_{0,i}^{tr}$ are listed in Appendix C. The rotation $\boldsymbol{R}$ considered corresponds to the 'A1–T1b' sample in the nomenclature of Shield (1995), and is given by

$$\boldsymbol{R} = \begin{bmatrix} 0.925 & 0.380. & 0 \\ -0.380 & 0.925 & 0 \\ 0 & 0 & 1 \end{bmatrix}$$

The thermo-mechanical response of the sample is obtained by solving the maximization problem (31) with a Broyden–Fletcher–Goldfarb–Shanno algorithm, using respectively the expressions (34) and (37) for evaluating J and an ascent direction. A finite-element method is used for discretizing (34) and (37) with respect to space. The mesh considered consists of 16 × 8 × 1 eight-node brick elements, as represented on Fig. 1. The problem (37) is linear and does not present any substantial difficulty. The nonlinear problem (34) is more delicate, notably because of the constraint (38) on the internal variable $\boldsymbol{\alpha}$. We use a method proposed in Peigney et al., 2011 for solving (34) in the presence of such constraints. That method essentially consists in reformulating (34) as a linear complementarity problem (via a change of variables) and from there using a interior-point algorithm (see e.g. the books by Ye (1997) or Wright (1997)) for a detailed presentation of linear complementarity problems and interior-point methods).

For CuAlNi, the results obtained with the boundary condition (i) and (ii) are qualitatively similar. The main difference is that fluctuations of the temperature are more pronounced for boundary condition (i). In the following we only present results corresponding to the boundary condition (i).

The evolution of the phase transformation during the loading is illustrated on Fig. 1 (top), along with the evolution of the temperature field (bottom). Those numerical results correspond to $h = 400\ \text{W.m}^{-2}.\text{K}^{-1}$, $\theta_R = 313$ K, $\dot{\varepsilon}^* = 2.10^{-3}\text{s}^{-1}$. In the free energy (39), the elasticity tensor $\boldsymbol{L}$ is taken as isotropic with a Young's modulus equal to 26.7 Gpa and a Poisson's ration equal to 0.25 (Shield, 1995; Govindjee and Miehe, 2001). The transformation temperature θ_T and the latent heat λ_T are set equal to 277 K and 46.7 Mpa, respectively. Those values have been measured by Shield (1995) using differential scanning calorimetry. The specific heat c is taken as 3.1 Mpa (Otsuka and Wayman, 1999). The components of the dissipative parameters $\boldsymbol{G}^+$ and $\boldsymbol{G}^-$ take a common value G that is identified from Shield's experiments and is equal to 0.15 Mpa (see Peigney et al., 2011 for more details).

As can be observed on Fig. 1, the phase transformation initiates at the middle section of the sample, and propagates towards the end sections. In order to explain that behaviour, note from (41) that the condition for (austenite to martensite) phase transformation to occur at point $\boldsymbol{x}$ and time t reads

$$\min_i \boldsymbol{\sigma}(\boldsymbol{x}, t) : \boldsymbol{\varepsilon}_i^{tr} = G + \frac{\lambda}{\theta_T}(\theta - \theta_T). \tag{44}$$

For small time t, the evolution is elastic (no phase transformation) and the temperature is equal to θ_R at all point. In such case, the

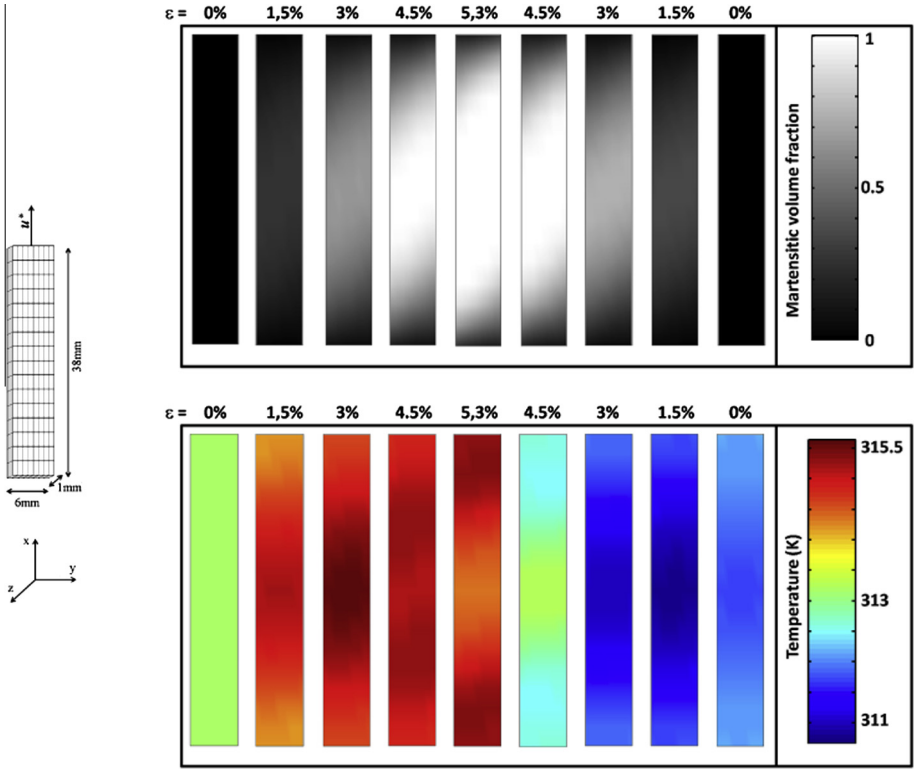

Fig. 1. Phase transformation (top) and temperature distribution (bottom) in a CuAlNi rectangular sample loaded in traction.

stress field $\boldsymbol{\sigma}(\boldsymbol{x},t)$ can be written as $(t/T)\boldsymbol{\sigma}^E(\boldsymbol{x})$ where $\boldsymbol{\sigma}^E(\boldsymbol{x})$ is solution of the following linear elasticity problem:

$$\begin{aligned} &\operatorname{div}\boldsymbol{\sigma}^E = 0, \quad \boldsymbol{\sigma}^E.\boldsymbol{n} = 0 \text{ on } S_{lat};\\ &\boldsymbol{\sigma}^E = \boldsymbol{L} : (\nabla\boldsymbol{u}^E + {}^T\nabla\boldsymbol{u}^E)/2;\\ &\boldsymbol{u}^E = 0 \text{ on } x = 0, \quad \boldsymbol{u}^E = u^{max}\boldsymbol{e}_x \text{ on } x = L. \end{aligned} \tag{45}$$

Because of the clamped boundary conditions at $x = 0$ and $x = L$, the stress field $\boldsymbol{\sigma}^E(\boldsymbol{x})$ is not homogeneous and exhibits some stress concentration near the end sections. From (44), phase transformation initiates at point $\boldsymbol{x}^*$ such that

$$\min_i \boldsymbol{\sigma}^E(\boldsymbol{x}^*) : \boldsymbol{\varepsilon}_i^{tr} = \sup_{\boldsymbol{x}\in\Omega}(\min_i \boldsymbol{\sigma}^E(\boldsymbol{x}) : \boldsymbol{\varepsilon}_i^{tr}). \tag{46}$$

In the case of CuAlNi, that condition is met at the middle section, even though the Von Mises stress at that location is lower than near the end sections.

The thermo-mechanical coupling results in a heterogeneous temperature field, the phase transformation front acting as a moving heat source in accordance with (42). The variations of the temperature with respect to the ambient temperature θ_R get more pronounced when the strain rate $\dot{\varepsilon}^*$ increases, as illustrated on Fig. 2. On that Figure are represented the maximum and minimum temperatures in the sample at $t = T$, i.e. when the applied strain is maximum. Variations of the temperature are of the order of 10 K for high strain rates, which is consistent with the order of magnitude observed experimentally (Grabe and Bruhns, 2008). Observe on Fig. 2 that θ^{max} and θ^{min} converge towards a limit as $\dot{\varepsilon}^* \to +\infty$. That behaviour can be explaining by noting that, for high values of $\dot{\varepsilon}^*$, conduction and convection effects become negligible compared to the latent heat effect. In such case, the local temperature $\theta(\boldsymbol{x},t)$ at point $\boldsymbol{x}$ and time t is directly correlated to the evolution of $\boldsymbol{\alpha}(\boldsymbol{x},t)$ at the same point. More precisely, using the simplifying assumption $G \ll (\theta/\theta_T)\lambda_T$, the integration of the heat Eq. (42) with respect to t gives

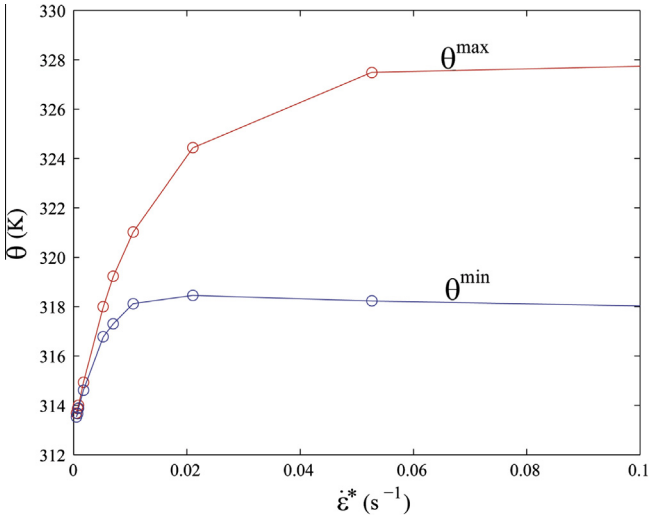

Fig. 2. Maximum and minimum temperatures in the sample as a function of the loading strain rate.

$$\theta(\boldsymbol{x},t) \simeq \theta_R \exp\left(\frac{\lambda_T}{c\theta_T}\left(\sum_{i=1}^{n}\alpha_i(\boldsymbol{x},t)\right)\right). \tag{47}$$

The temperature is thus maximum at points $\boldsymbol{x}$ where the material is fully transformed in martensite, i.e. at points where $\sum_i \alpha_i(\boldsymbol{x},t) = 1$. It follows that

$$\theta^{max} = \theta_R \exp\left(\frac{\lambda_T}{c\theta_T}\right). \tag{48}$$

For the material parameters of CuAlNi, the formula (48) gives $\theta^{max} = 330.7$ K. The simulation results for $\dot{\varepsilon} = 0.5$ gives

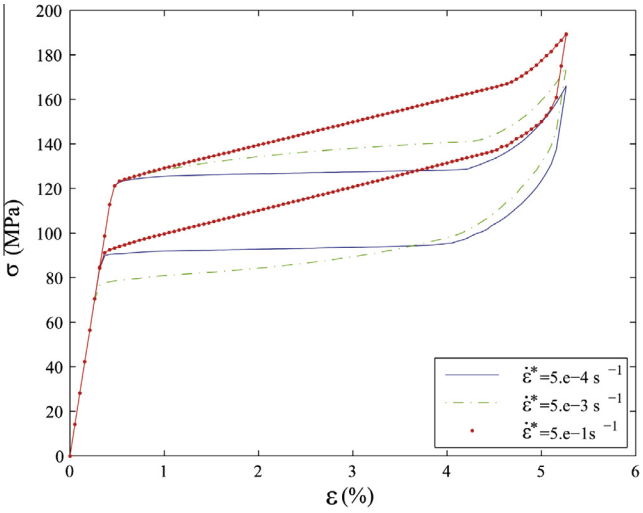

Fig. 3. Stress–strain curves at several applied strain rates (CuAlNi).

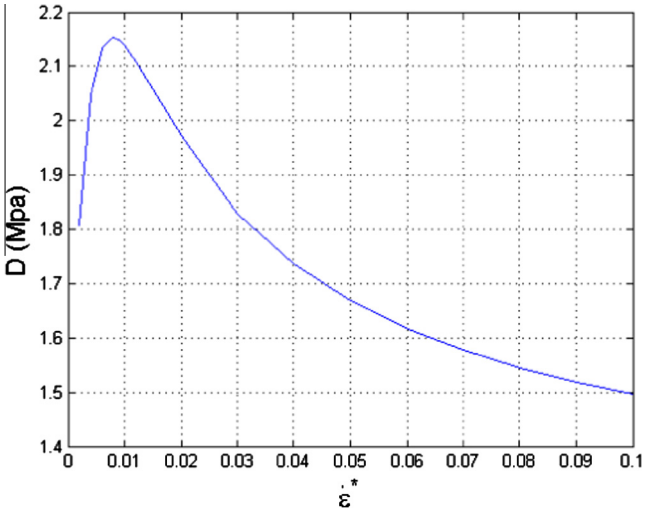

Fig. 4. Size of the hysteresis loop as a function of the loading strain rate.

$\theta^{max} = 330.6$ K, which is in good agreement with (48). A formula analog to (48) holds for θ^{min}: using (47) we have

$$\theta^{min} = \theta_R \exp\left(\frac{\lambda_T}{c\theta_T} \min_{\boldsymbol{x}\in\Omega}\left(\sum_{i=1}^{n}\alpha_i(\boldsymbol{x},T)\right)\right). \tag{49}$$

However, at time $t = T$, phase transformation is initiated at all point in the sample, i.e. $\sum_i \alpha_i(\boldsymbol{x},T) > 0$ for all $\boldsymbol{x}$. The minimum value $\min_{\boldsymbol{x}}\sum_i \alpha_i(\boldsymbol{x},T)$ is non zero and cannot be obtained in closed form. For $\dot{\varepsilon}^* = 0.5$, the numerical simulation gives $\min_{\boldsymbol{x}}\sum_i \alpha_i(\boldsymbol{x},T) = 0.163$ and $\theta^{min} = 315.9$ K. Those values are compatible with (47).

On Fig. 3 are represented the stress–strain curves obtained for several values of the applied strain rate $\dot{\varepsilon}^*$. The curve obtained for a very low strain rate ($\dot{\varepsilon}^* = 5.10^{-4}$ s^{-1}) coincides with the isothermal simulations presented in Peigney et al. (2011) and exhibits some distinctive plateaux in the stress response. As the applied strain rate $\dot{\varepsilon}^*$ is increased, some hardening of the stress–strain curve is observed. As can be noticed on Fig. 3, the hardening is strain-rate dependent. That behaviour is a direct consequence of thermal effects. Let us indeed emphasize that the mechanical behaviour of the model is rate-independent: the only parameters that introduce a time scale are those related to thermal effects (thermal conduction K, convection coefficient h, specific heat c).

The size of the hysteresis loop (here denoted by $\mathcal{D}$) is an important parameter in some applications of shape-memory alloys, such as damping applications. There are contradictory experimental observations in the literature concerning the variation of $\mathcal{D}$ with respect to the applied strain-rate $\dot{\varepsilon}^*$. Some authors, as Shaw and Kyriakides (1997) observe that $\mathcal{D}$ increases with the applied strain rate, whereas others, as Dolce and Cardone (2001), observe the opposite. In the present model, $\mathcal{D}$ varies in a non monotonic fashion with $\dot{\varepsilon}^*$, as can be noted on Fig. 3. This is shown more clearly on Fig. 4: $\mathcal{D}$ increases for low value of $\dot{\varepsilon}^*$ and then decreases after having reached a maximum. The maximum value of $\mathcal{D}$ as well as the corresponding value of $\dot{\varepsilon}^*$ are not intrinsic properties of the material: they depend on the surrounding medium (notably through the convection coefficient h) as well as on the shape and dimensions of the sample. Provided such a behaviour is not just an artefact of the model and corresponds to a real phenomenon, it would explain the seemingly contradictory observations found in the literature.

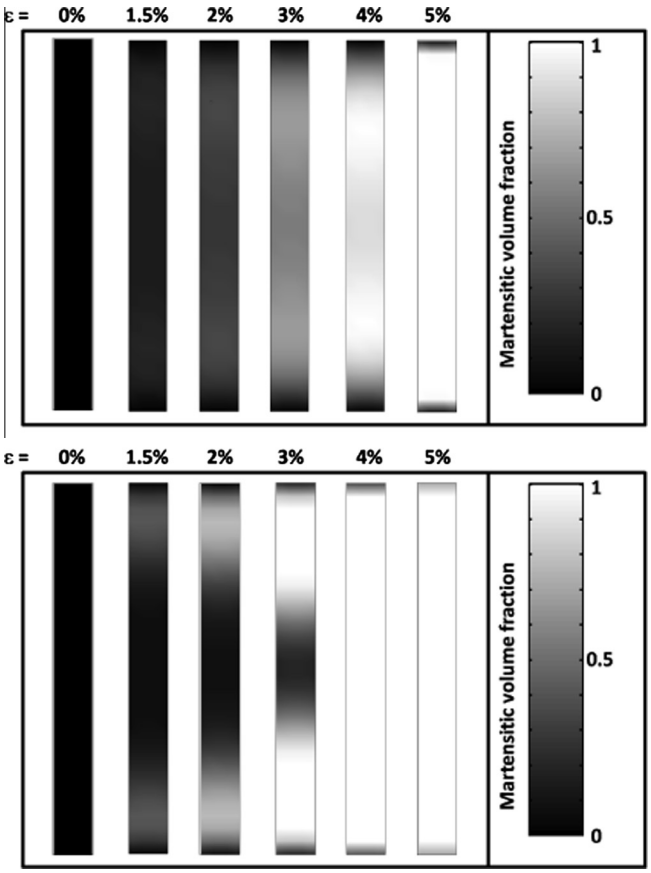

Fig. 5. Phase transformation in NiTi, for two different thermal boundary conditions at the end sections: null heat flux (top) and prescribed temperature (bottom).

5.2. Influence of the thermal boundary conditions

We now consider an example related to NiTi alloys. As detailed in Appendix C, there are twelve transformation strains to be considered for that material. The geometry and the mechanical boundary conditions are identical to those considered previously for CuAlNi, except that the dimensions of the sample are now 15 mm × 2 mm × 0.3 mm.

On Fig. 5 is presented the phase transformation evolution obtained from the two types of boundary conditions (*i*) and (*ii*). The thermal boundary condition (*ii*) results in a clearer localization of the phase transformation: for sufficiently high values of $\dot{\varepsilon}$, phase transformation initiates at the end sections and propagates towards the middle section. That last scenario is in agreement with the numerical simulations performed by Anand and Gurtin (2003) for the same material and geometry, with a boundary condition of type (*ii*). Recall that phase transformation initiates at points $\boldsymbol{x}$ satisfying the condition (46). That condition strongly depends on the transformation strains in the alloy considered. In the case of NiTi, the condition (46) is satisfied near the end sections, in contrast with the CuAlNi example considered previously. The time t^* when phase transformation begins is given by

$$\frac{t^*}{T}\min_i \boldsymbol{\sigma}^E(\boldsymbol{x}^*) : \boldsymbol{\varepsilon}_i^{tr} = G. \tag{50}$$

Note that (46) and (50) are independent on the thermal boundary conditions. The initiation of phase-transformation is thus identical for both boundary conditions (*i*) and (*ii*). As soon as phase transformation begins, heat is produced and the temperature rises locally. This is when the thermal boundary condition matters. Observe from (44) that high temperatures defavour phase transformation. In the vicinity of the end sections, the adiabatic boundary condition (*i*) tends to keep the temperature high compared to the fixed temperature boundary condition (*ii*). In such condition, phase transformation becomes favoured near the middle sections, where the temperature remains close to θ_R. On the contrary, compared to the condition $\boldsymbol{q} = 0$ used in (*i*), the boundary condition (*ii*) helps in preventing significant rise of the temperature near the end sections and therefore promotes phase transformation in those points.

The strain–stress curves obtained for the boundary conditions (*i*) and (*ii*) are represented on Fig. 6. Although the loading strain rate ($\dot{\varepsilon}^* = 10^{-3}\mathrm{s}^{-1}$) is the same for both simulations, the obtained stress–strain curves are dramatically different. The thermal boundary condition (*i*) results in a larger hardening of the response compared to (*ii*). Also note that the stress–strain curve for boundary condition (*ii*) is linear for $\varepsilon > 4\%$, which indicates that phase transformation in martensite is complete for such level of strains. For both boundary conditions, the size $\mathcal{D}$ of the hysteresis loop is bigger than for the isothermal case (represented as dashed lines on Fig. 6). In accordance with (46)–(50), the phase transformation begins for the same applied strain (about 0.76%) on the three responses.

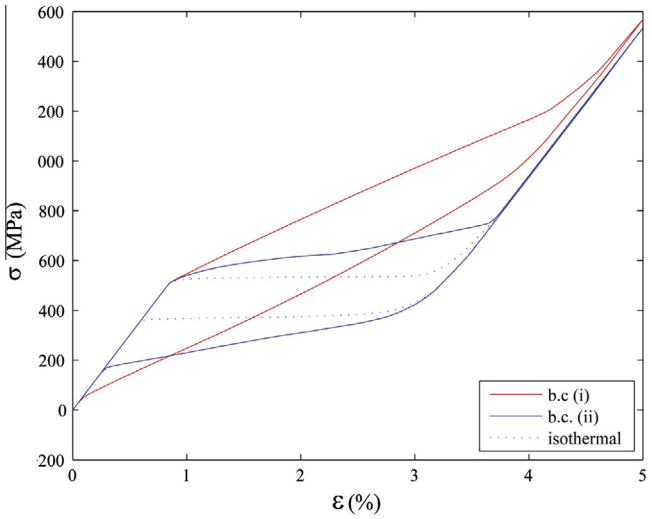

Fig. 6. Stress–strain curves in NiTi for different thermal conditions.

The results of Figs. 5,6 show that phase transformation may strongly depend on the thermal boundary condition. Such an effect is not observed on the CuAlNi example considered previously. The reason is that the phase transformation in CuAlNi initiates at the middle section (see Fig. 1), so that the thermal boundary conditions at the end sections do not have as strong an impact.

6. Concluding remarks

In this paper have been studied some incremental variational principles for the thermo-mechanical problem that results from the combination of generalized standard materials, non-smooth mechanics, and Fourier's law. Compared to the isothermal case, existence of solution is obtained under the additional requirement that the Helmholtz free energy w is concave with respect to the temperature. Building on those incremental variational principles, it has been shown that the incremental thermo-mechanical problem could be recast as a concave maximization problem. Although other routes are possible for solving the incremental problem, that particular way has the attractive feature of being simple to implement. Indeed the problem ultimately reduces to a sequence of linear scalar problems and purely mechanical problems, defined respectively by (34) and (37). Note that the structure of the linear scalar problem (37) to solve is independent on the material model considered (i.e. on the expression of the free energy w and of the dissipation potential Φ). All the specificities of the material model appear in the purely mechanical problem (34), which has the same structure as the incremental problem supplied by the Euler implicit scheme in the isothermal case. This is also where all the difficulties are concentrated, as nonlinearities, non-differentiabilities and constraints on the state variables may need to be handled. Provided one can solve that isothermal problem, the thermo-mechanical problem can be solved with low additional effort in terms of numerical implementation. For the micromechanical model of shape-memory alloys considered in Section 5, the isothermal algorithm proposed by Peigney et al. (2011) acted as a building block for the thermo-mechanical simulations. Such simulations are important for the design of SMA-based systems, as instance for estimating the response-time of SMA actuators, or for assessing the energy absorption capability of SMA dampers. Shape-memory alloys are obviously just an example of possible applications of the proposed approach, which for instance could be used for a wide class of plasticity models. In this paper, some mathematical aspects have been kept at a formal level. For instance, the choice of functional spaces for the different fields considered has not been discussed in detail. It would be interesting to explore those aspects in a more thorough full fashion, notably in order to study the convergence of solutions as the time increment tends towards zero.

Appendix A. Derivation of the variational principle for the incremental thermo-mechanical problem

In this section, we establish that solutions of the variational problem (29) are solutions of the incremental thermo-mechanical problem (27). Studying the stationarity conditions with respect to $\boldsymbol{u}$ and $\boldsymbol{\alpha}$ in is similar to the isothermal case (29) and leads to (27.1)–(27.3). In the following we focus on the stationarity condition with respect to θ. For any $\tilde{\theta}$ such that $\tilde{\theta} = 0$ on Γ_θ, we have

$$\frac{\partial \mathcal{F}}{\partial \theta}.\tilde{\theta} = \frac{\partial \mathcal{F}^\theta}{\partial \theta}.\tilde{\theta} + \int_\Omega \left(-s + \frac{1}{\theta^0}\Phi(\boldsymbol{\alpha} - \boldsymbol{\alpha}^0)\right)\tilde{\theta}\, d\omega \tag{A.1}$$

where

$$\frac{\partial \mathcal{F}^\theta}{\partial \theta}.\tilde{\theta} = \int_\Omega \left[s^0 + \delta t \frac{r}{\theta^0} + K\delta t \left(\frac{\|\nabla \theta^0\|}{\theta^0} \right)^2 \right] \tilde{\theta}\, d\omega - \int_\Omega K\delta t \times \frac{\nabla\theta}{\theta^0} \nabla\tilde{\theta}\, d\omega - \delta t \int_{\Gamma_q} \frac{q^d}{\theta^0}\tilde{\theta}\, da - h\delta t \int_{\Gamma_h} \frac{(\theta-\theta_R)}{\theta^0}\tilde{\theta}\, da. \quad (A.2)$$

Integrating by part gives the identity

$$-\int_\Omega \frac{\nabla\theta}{\theta^0}.\nabla\tilde{\theta}\, d\omega = \int_\Omega \tilde{\theta}\nabla\left(\frac{\nabla\theta}{\theta^0}\right) d\omega - \int_{\partial\Omega} \frac{\nabla\theta.\boldsymbol{n}}{\theta^0}\tilde{\theta}\, da$$

with

$$\nabla\left(\frac{\nabla\theta}{\theta^0}\right) = \frac{\Delta\theta}{\theta^0} - \frac{\nabla\theta^0.\nabla\theta}{(\theta^0)^2}.$$

Therefore

$$\frac{\partial \mathcal{F}^\theta}{\partial \theta}.\tilde{\theta} = \int_\Omega \left[\theta^0 s^0 + r\delta t + K\delta t \left(\frac{\|\nabla\theta^0\|^2}{\theta^0} - \frac{\nabla\theta.\nabla\theta^0}{\theta^0} + \Delta\theta \right) \right] \frac{\tilde{\theta}}{\theta^0} d\omega - \delta t \int_{\Gamma_q} \frac{q^d + K\nabla\theta.n}{\theta^0}\tilde{\theta}\, da - \delta t \int_{\Gamma_h} \times \frac{h(\theta-\theta_R) + K\nabla\theta.n}{\theta^0}\tilde{\theta}\, da. \quad (A.3)$$

Moreover, since Φ is positively homogeneous of degree 1 and $\boldsymbol{A}^d \in \partial\Phi(\boldsymbol{\alpha}-\boldsymbol{\alpha}^0)$, we have $(\lambda-1)\Phi(\boldsymbol{\alpha}-\boldsymbol{\alpha}^0) = \Phi(\lambda(\boldsymbol{\alpha}-\boldsymbol{\alpha}^0)) - \Phi(\boldsymbol{\alpha}-\boldsymbol{\alpha}^0) \geqslant (\lambda-1)\boldsymbol{A}^d.(\boldsymbol{\alpha}-\boldsymbol{\alpha}^0)$ for any $\lambda \geqslant 0$. This implies that

$$\Phi(\boldsymbol{\alpha}-\boldsymbol{\alpha}^0) = \boldsymbol{A}^d.(\boldsymbol{\alpha}-\boldsymbol{\alpha}^0). \quad (A.4)$$

Substituting (A.3),(A.4) in (A.1) we obtain

$$\frac{\partial \mathcal{F}}{\partial \theta}.\tilde{\theta} = \int_\Omega \left[\theta^0(s^0 - s) + r\delta t + \boldsymbol{A}^d.(\boldsymbol{\alpha}-\boldsymbol{\alpha}^0) + K\delta t \left(\frac{\|\nabla\theta^0\|^2}{\theta^0} - \frac{\nabla\theta.\nabla\theta^0}{\theta^0} + \Delta\theta \right) \right] \frac{\tilde{\theta}}{\theta^0} d\omega - \delta t \int_{\Gamma_q} \frac{q^d + K\nabla\theta.n}{\theta^0}\tilde{\theta}\, da - \delta t \int_{\Gamma_h} \frac{h(\theta-\theta_R) + K\nabla\theta.n}{\theta^0}\tilde{\theta}\, da. \quad (A.5)$$

Therefore, the stationarity condition $\partial\mathcal{F}/\partial\theta = 0$ give the relations (27.4),(27.5).

Appendix B. Directional derivative of J

Assuming that w is convex in $(\boldsymbol{u},\boldsymbol{\alpha})$ and concave in θ, let us establish that the function J in (32) is concave. A first observation is that $\mathcal{F}^\theta, \mathcal{F}^e$ as well as $\mathcal{F}^d$ are concave with respect to θ. In (32), the term $\min_{(\boldsymbol{u},\boldsymbol{\alpha})}\{\mathcal{F}^e(\boldsymbol{u},\boldsymbol{\alpha},\theta) + \mathcal{F}^d(\boldsymbol{\alpha},\theta)\}$ is the minimum of a family of concave functions (parametrized by $(\boldsymbol{u},\boldsymbol{\alpha})$), and therefore is concave in θ. As a result, the function J in (32) is concave. The concavity of J implies the existence of the directional derivative

$$DJ(\theta;\tilde{\theta}) = \lim_{t\to 0^+} \frac{J(\theta(t)) - J(\theta)}{t}$$

where $\theta(t) = \theta + t\tilde{\theta}$ and $\tilde{\theta}$ vanished on Γ_θ. We prove in the following that $DJ(\theta;\tilde{\theta})$ satisfied the inequality (35). To that purpose, let us denote by $(\boldsymbol{u}(t),\boldsymbol{\alpha}(t))$ the solution of the minimization problem

$$\min_{(\boldsymbol{u},\boldsymbol{\alpha})\in\mathcal{K}_u\times\mathcal{K}_\alpha} \{\mathcal{F}^e(\boldsymbol{u},\boldsymbol{\alpha},\theta(t)) + \mathcal{F}^d(\boldsymbol{\alpha},\theta(t))\}$$

so that

$$J(\theta(t)) = \mathcal{F}^\theta(\theta(t)) + \mathcal{F}^e(\boldsymbol{u}(t),\boldsymbol{\alpha}(t),\theta(t)) + \mathcal{F}^d(\boldsymbol{\alpha}(t),\theta(t)). \quad (B.1)$$

From the definition of $(\boldsymbol{u}(t),\boldsymbol{\alpha}(t))$ we obtain

$$\mathcal{F}^e(\boldsymbol{u}(t),\boldsymbol{\alpha}(t),\theta) + \mathcal{F}^d(\boldsymbol{\alpha}(t),\theta) \geqslant \mathcal{F}^e(\boldsymbol{u}(0),\boldsymbol{\alpha}(0),\theta) + \mathcal{F}^d(\boldsymbol{\alpha}(0),\theta). \quad (B.2)$$

Combining (B.1) and (B.2) yields

$$J(\theta(t)) - J(\theta) \geqslant [\mathcal{F}^e(\boldsymbol{u}(t),\boldsymbol{\alpha}(t),\theta(t)) - \mathcal{F}^e(\boldsymbol{u}(t),\boldsymbol{\alpha}(t),\theta)] + [\mathcal{F}^d(\boldsymbol{\alpha}(t),\theta(t)) - \mathcal{F}^d(\boldsymbol{\alpha}(t),\theta)] + [\mathcal{F}^\theta(\theta(t)) - \mathcal{F}^\theta(\theta)]. \quad (B.3)$$

We now examine the limits (as $t\to 0^+$) of the three terms in brackets in the right-hand side of (B.3). The expression (22) of $\mathcal{F}^e$ gives

$$\frac{\mathcal{F}^e(\boldsymbol{u}(t),\boldsymbol{\alpha}(t),\theta(t)) - \mathcal{F}^e(\boldsymbol{u}(t),\boldsymbol{\alpha}(t),\theta)}{t} \underset{t\to 0^+}{\to} \int_\Omega \frac{\partial w}{\partial\theta}\tilde{\theta}\, d\omega \quad (B.4)$$

where $\partial w/\partial\theta$ is evaluated at $(\boldsymbol{u}(0),\boldsymbol{\alpha}(0),\theta)$. Moreover, we have

$$\frac{\mathcal{F}^\theta(\theta(t)) - \mathcal{F}^\theta(\theta^*)}{t} \underset{t\to 0^+}{\to} \frac{\partial\mathcal{F}^\theta}{\partial\theta}.\tilde{\theta} \quad (B.5)$$

where the expression of $(\partial\mathcal{F}^\theta/\partial\theta).\tilde{\theta}$ is given in (A.2). Since $\mathcal{F}^d$ is linear with respect to θ, we obtain

$$\frac{\mathcal{F}^d(\boldsymbol{\alpha}(t),\theta(t)) - \mathcal{F}^d(\boldsymbol{\alpha}(t),\theta)}{t} = \int_\Omega \tilde{\theta}\Phi(\boldsymbol{\alpha}(\boldsymbol{x},t))d\omega \underset{t\to 0^+}{\to} \int_\Omega \tilde{\theta}\Phi(\boldsymbol{\alpha}(\boldsymbol{x},0))d\omega. \quad (B.6)$$

Substituting (B.4)–(B.6) in (B.3), we obtain

$$DJ(\theta,\tilde{\theta}) \geqslant D\mathcal{F}^\theta(\theta,\tilde{\theta}) + \int_\Omega (-s + \boldsymbol{A}^d.(\boldsymbol{\alpha}-\boldsymbol{\alpha}^0))\tilde{\theta}\, d\omega \quad (B.7)$$

where the definition $s = -\partial w/\partial\theta$ and the relation $\Phi(\boldsymbol{\alpha}-\boldsymbol{\alpha}^0) = \boldsymbol{A}^d.(\boldsymbol{\alpha}-\boldsymbol{\alpha}^0)$ have been used. Comparing with (A.5) shows that the right-hand side of (B.7) is equal to $(\partial\mathcal{F}/\partial\theta).\tilde{\theta}$. We thus obtain

$$DJ(\theta,\tilde{\theta}) \geqslant \frac{\partial\mathcal{F}}{\partial\theta}.\tilde{\theta}$$

Appendix C. Transformation strains in CuAlNi and NiTi

The CuAlNi alloy obeys a cubic to orthorombic transformation, for which there are 6 (lattice correspondent) martensitic variants with reference transformation strains given by

$$\boldsymbol{\varepsilon}^{tr}_{0,1} = \begin{bmatrix} \alpha & 0 & \delta \\ 0 & \beta & 0 \\ \delta & 0 & \alpha \end{bmatrix}, \quad \boldsymbol{\varepsilon}^{tr}_{0,2} = \begin{bmatrix} \alpha & 0 & -\delta \\ 0 & \beta & 0 \\ -\delta & 0 & \alpha \end{bmatrix},$$

$$\boldsymbol{\varepsilon}^{tr}_{0,3} = \begin{bmatrix} \alpha & \delta & 0 \\ \delta & \alpha & 0 \\ 0 & 0 & \beta \end{bmatrix}, \quad \boldsymbol{\varepsilon}^{tr}_{0,4} = \begin{bmatrix} \alpha & -\delta & 0 \\ -\delta & \alpha & 0 \\ 0 & 0 & \beta \end{bmatrix}, \quad (C.1)$$

$$\boldsymbol{\varepsilon}^{tr}_{0,5} = \begin{bmatrix} \beta & 0 & 0 \\ 0 & \alpha & \delta \\ 0 & \delta & \alpha \end{bmatrix}, \quad \boldsymbol{\varepsilon}^{tr}_{0,6} = \begin{bmatrix} \beta & 0 & 0 \\ 0 & \alpha & -\delta \\ 0 & -\delta & \alpha \end{bmatrix}.$$

For CuAlNi, values of the lattice parameters are $\alpha = 0.0425, \beta = -0.0822, \delta = 0.0194$ (Chu, 1993).

In the case of NiTi, austenite and martensite respectively have a cubic and monoclinic-I structure. There are 12 martensitic variants, with transformation strains given by:

$$
\begin{aligned}
\boldsymbol{\varepsilon}^{tr}_{0,1} &= \begin{bmatrix} \alpha & \delta & \epsilon \\ \delta & \alpha & \epsilon \\ \epsilon & \epsilon & \beta \end{bmatrix}, \quad \boldsymbol{\varepsilon}^{tr}_{0,2} = \begin{bmatrix} \alpha & \delta & -\epsilon \\ \delta & \alpha & -\epsilon \\ -\epsilon & -\epsilon & \beta \end{bmatrix}, \\
\boldsymbol{\varepsilon}^{tr}_{0,3} &= \begin{bmatrix} \alpha & -\delta & -\epsilon \\ -\delta & \alpha & \epsilon \\ -\epsilon & \epsilon & \beta \end{bmatrix}, \quad \boldsymbol{\varepsilon}^{tr}_{0,4} = \begin{bmatrix} \alpha & -\delta & \epsilon \\ -\delta & \alpha & -\epsilon \\ \epsilon & -\epsilon & \beta \end{bmatrix}, \\
\boldsymbol{\varepsilon}^{tr}_{0,5} &= \begin{bmatrix} \alpha & \epsilon & \delta \\ \epsilon & \beta & \epsilon \\ \delta & \epsilon & \alpha \end{bmatrix}, \quad \boldsymbol{\varepsilon}^{tr}_{0,6} = \begin{bmatrix} \alpha & -\epsilon & \delta \\ -\epsilon & \beta & -\epsilon \\ \delta & -\epsilon & \alpha \end{bmatrix}, \\
\boldsymbol{\varepsilon}^{tr}_{0,7} &= \begin{bmatrix} \alpha & -\epsilon & -\delta \\ -\epsilon & \beta & \epsilon \\ -\delta & \epsilon & \alpha \end{bmatrix}, \quad \boldsymbol{\varepsilon}^{tr}_{0,8} = \begin{bmatrix} \alpha & \epsilon & -\delta \\ \epsilon & \beta & -\epsilon \\ -\delta & -\epsilon & \alpha \end{bmatrix}, \\
\boldsymbol{\varepsilon}^{tr}_{0,9} &= \begin{bmatrix} \beta & \epsilon & \epsilon \\ \epsilon & \alpha & \delta \\ \epsilon & \delta & \alpha \end{bmatrix}, \quad \boldsymbol{\varepsilon}^{tr}_{0,10} = \begin{bmatrix} \beta & -\epsilon & -\epsilon \\ -\epsilon & \alpha & \delta \\ -\epsilon & \delta & \alpha \end{bmatrix}, \\
\boldsymbol{\varepsilon}^{tr}_{0,11} &= \begin{bmatrix} \beta & -\epsilon & \epsilon \\ -\epsilon & \alpha & -\delta \\ \epsilon & -\delta & \alpha \end{bmatrix}, \quad \boldsymbol{\varepsilon}^{tr}_{0,12} = \begin{bmatrix} \beta & \epsilon & -\epsilon \\ \epsilon & \alpha & -\delta \\ -\epsilon & -\delta & \alpha \end{bmatrix}
\end{aligned}
\tag{C.2}
$$

For nearly equiatomic NiTi alloys, the values of the lattice parameters are $\alpha = 0.0243, \beta = -0.0437, \delta = 0.058, \epsilon = 0.0427$ (Knowles and Smith, 1981).

References

Abeyaratne, R., Kim, S., Knowles, J., 1994. A one-dimensional continuum model for shape-memory alloys. Int. J. Solids Struct. 31, 2229–2249.

Anand, L., Gurtin, M., 2003. Thermal effects in the superelasticity of crystalline shape-memory materials. J. Mech. Phys. Solids 51 (6), 1015–1058.

Auricchio, F., Petrini, L., 2004. A three-dimensional model describing stress-temperature induced solid phase transformations, part II: thermomechanical coupling and hybrid composite applications. Int. J. Numer. Methods Eng. 61, 716–737.

Bhattacharya, K., 1993. Comparison of the geometrically nonlinear and linear theories of martensitic transformation. Cont. Mech. Thermodyn. 5, 205–242.

Bhattacharya, K. Microstructure of Martensite, Oxford Series on Materials Modelling, Oxford materials edn., 2003.

Brézis, H., 1972. Opérateurs maximum monotones et semigroupes de contractions dans les espaces de Hilbert. North-Holland, Amsterdam.

Bui, H., 2006. Fracture Mechanics, Inverse Problems and Solution. Springer.

Chrysochoos, A., Licht, C., Peyroux, R., 2003. A one-dimensional thermomechanical modeling of phase change front propagation in a SMA monocrystal. C.R. Mecanique 331, 25–32.

Chu, C. Hysteresis and microstructures: a study of biaxial loading on compound twins of copper-aluminium-nickel single crystals, Ph.D. thesis, University of Minnesota, Minneapolis, 1993.

Dacorogna, B., 2008. Direct Methods in the Calculus of Variations. Springer.

Dolce, M., Cardone, D., 2001. Mechanical behaviour of SMA for seismic applications. 2: austenite NiTi wires subjects in tension. Int. J. Mech. Sci. 43, 2656–2677.

Frémond, M., 2002. Non Smooth Thermo-mechanics. Springer.

Govindjee, S., Miehe, C., 2001. A multi-variant martensitic phase transformation model: formulation and numerical implementation. Comput. Mech. Appl. Mech. Eng. 191, 215–238.

Grabe, C., Bruhns, O., 2008. On the viscous and strain rate dependant behavior of polycrystalline NiTi. Int. J. Solids Struct. 45, 1876–1895.

Hackl, K., Heinen, R., 2008. An upper bound to the free energy of n-variant polycrystalline shape memory alloys. J. Mech. Phys. Solids 56, 2832–2843.

Halphen, B., Nguyen, Q., 1975. Sur les matériaux standards généralisés. J. Mécanique 14, 1–37.

Knowles, K., Smith, D., 1981. Crystallography of the martensitic transformation in equiatomic nickel–titanium. Acta Mater. 29, 101–110.

Lahellec, N., Suquet, P., 2007. On the effective behavior of nonlinear inelastic composites: I. Incremental variational principles. J. Mech. Phys. Solids 55, 1932–1963.

Lions, J., 1968. Contrôle optimal de systèmes gouvernés par des équations aux dérivées partielles. Dunod.

Miehe, C., 2002. Strain-driven homogenization of inelastic microstructures and composites based on an incremental variational formulation. Int. J. Numer. Methods Eng. 55, 1285–1322.

Miehe, C., Lambrecht, M., Gürses, E., 2004. Analysis of material instabilities in inelastic solids by incremental energy minimization and relaxation methods: evolving deformation microstructures in finite plasticity. J. Mech. Phys. Solids 52, 2725–2769.

Moreau, J., Panagiotopoulos, P., 1988. Nonsmooth Mechanics and Applications. Springer.

Ortiz, M., Repetto, E., 1999. Nonconvex energy minimization and dislocation structures in ductile single crystals. J. Mech. Phys. Solids 47, 397–462.

Ortiz, M., Stainier, L., 1999. The variational formulation of viscoplastic constitutive updates. Comput. Mech. Appl. Mech. Eng. 171, 419–444.

Otsuka, K., Wayman, C., 1999. Shape Memory Materials. Cambridge University Press.

Peigney, M., 2006. A time-integration scheme for thermomechanical evolutions of shape-memory alloys. C. R. Mecanique 334, 266–271.

Peigney, M., 2009. A non-convex lower bound on the effective free energy of polycrystalline shape memory alloys. J. Mech. Phys. Solids 57, 970–986.

Peigney, M., 2010. Shakedown theorems and asymptotic behaviour of solids in non-smooth mechanics. Eur. J. Mech. A 29, 785–793.

Peigney, M., 2013a. On the energy-minimizing strains in martensitic microstructures – Part 1: geometrically nonlinear theory. J. Mech. Phys. Solids, 1486–1510.

Peigney, M., 2013b. On the energy-minimizing strains in martensitic microstructures – Part 2: geometrically linear theory. J. Mech. Phys. Solids, 1511–1530.

Peigney, M., Stolz, C., 2001. Approche par contrôle optimal des structures élastoviscoplastiques sous chargement cyclique. C. R. Acad. Sci Paris II b 329, 643–648.

Peigney, M., Stolz, C., 2003. An optimal control approach to the analysis of inelastic structures under cyclic loading. J. Mech. Phys. Solids 51, 575–605.

Peigney, M., Seguin, J., Hervé-Luanco, E., 2011. Numerical simulation of shape memory alloys structures using interior-point methods. Int. J. Solids Struct. 48, 2791–2799.

Peyroux, R., Chrysochoos, A., Licht, C., Löbel, M., 1998. Thermomechanical couplings and pseudoelasticity of shape memory alloys. Int. T. Eng. Sci. 36, 489–509.

Rockafellar, R.T., 1970. Convex Analysis. Princeton University Press.

Shaw, J., Kyriakides, S., 1997. On the nucleation and propagation of phase transformation fronts in a NiTi alloy. Acta Mater. 45 (2), 683–700.

Shield, T., 1995. Orientation dependance of the pseudoelastic behaviour of single crystals of Cu–Al–Ni in tension. J. Mech. Phys. Solids 43 (6), 869–895.

Stolz, C., 2008. Optimal control approach in nonlinear mechanics. C.R. Mecanique 336, 238–244.

Wright, S., 1997. Primal-dual interior-point methods. Society for Industrial and, Applied Mathematics.

Yang, Q., Stainier, L., Ortiz, M., 2006. A variational formulation of the coupled thermo-mechanical boundary-value problem for general dissipative solids. J. Mech. Phys. Solids 54 (2), 401–424.

Ye, Y., 1997. Interior Point Algorithms: Theory and Analysis. Wiley Interscience.